



Sonoma Technology, Inc.

1360 Redwood Way, Suite C
Petaluma, CA 94954
707/665-9900
FAX 707/665-9800
www.sonomatech.com

**AN INVESTIGATION OF CAM_x MODELING
ISSUES WITH SENSITIVITY SIMULATIONS
FOR THE SEPTEMBER 6-11, 1993
OZONE EPISODE IN THE
HOUSTON-GALVESTON AREA**

**Final Report
STI-901303-2121-FR**

By:

**Neil J. M. Wheeler
Jason A. Roney
Sonoma Technology, Inc.
1360 Redwood Way, Suite C
Petaluma, CA 94954-1169**

**Kit K. Wagner
Atmospheric Information Systems
P.O. Box 721165
Norman, OK 73070**

**Prepared for:
Texas Natural Resource Conservation Commission
P.O. Box 13087
Austin, Texas 8711-3087**

August 31, 2001

TABLE OF CONTENTS

<u>Section</u>	<u>Page</u>
LIST OF FIGURES	v
LIST OF TABLES	ix
1. INTRODUCTION.....	1-1
2. METHODOLOGY	2-1
2.1 Sensitivity Simulations.....	2-1
2.1.1 Sensitivity 1 – Zero NO _x at W.A. Parish Power Plant	2-2
2.1.2 Sensitivity 2 – Domain-Wide 50% NO _x Reduction	2-2
2.1.3 Sensitivity 3 – 50% NO _x Reduction without W.A. Parish Power Plant.....	2-3
2.1.4 Sensitivity 4 – Zero NO _x in the Houston Ship Channel	2-3
2.1.5 Sensitivity 5 – Cloud Cover	2-3
2.1.6 Sensitivity 6 – Zero NO _x in Central Houston.....	2-6
2.1.7 Sensitivity 7 – Continuous Emission Upset	2-7
2.1.8 Sensitivity 8 – 50% NO _x Reduction with Cloud Cover	2-7
2.1.9 Sensitivity 9 – Enhanced Ship Channel Emissions of Ethene and Propene	2-7
2.1.10 Sensitivity 10 and 11 – Reduced Transport and Diffusion	2-8
2.1.11 Sensitivity 12 – Limited Duration Emissions Upset	2-8
1.2 Spike Intensity Calculation	2-8
3. RESULTS.....	3-1
3.1 Sensitivity Simulations.....	3-1
3.2 Cloud Cover Effects	3-26
3.3 Spike Intensity.....	3-31
4. DISCUSSION	4-1
4.1 Source Contributions to Peak Ozone Concentrations	4-1
4.2 Transport and Diffusion	4-1
4.3 Cloud Cover Effects	4-2
4.4 Simulation of Upsets	4-2
4.5 Simulation of Spike Intensity	4-2
5. CONCLUSIONS AND RECOMMENDATIONS.....	5-1
6. REFERENCES.....	6-1

LIST OF FIGURES

<u>Figure</u>	<u>Page</u>
2-1. Coverage of the SuperCOAST domain.	2-2
2-2. Initial satellite image.	2-5
2-3. Satellite image after threshold processing.	2-5
2-4. Final satellite image after artifact removal.	2-6
2-6. Spike analysis region.	2-9
3-1. Arrangement of sensitivity simulation figures.	3-1
3-2. S1 results for September 8, 1993: (a) peak ozone concentration for base; (b) peak ozone concentration for sensitivity at base; (c) peak time ozone concentration difference (sensitivity-base) at peak hour for base; (d) and ozone concentration difference (sensitivity-base) at hour of maximum difference.	3-2
3-3. S1 results for September 10, 1993: (a) peak ozone concentration for base; (b) peak ozone concentration for sensitivity at base peak time; (c) ozone concentration difference (sensitivity-base) at peak hour for base; and (d) ozone concentration difference (sensitivity-base) at hour of maximum difference.	3-3
3-4. S2 results for September 8, 1993: (a) peak ozone concentration for base; (b) peak ozone concentration for sensitivity at base peak time; (c) ozone concentration difference (sensitivity-base) at peak hour for base; and (d) ozone concentration difference (sensitivity-base) at hour of maximum difference.	3-4
3-5. S2 results for September 10, 1993: (a) peak ozone concentration for base; (b) peak ozone concentration for sensitivity at base peak time; (c) ozone concentration difference (sensitivity-base) at peak hour for base; and (d) ozone concentration difference (sensitivity-base) at hour of maximum difference.	3-5
3-6. S3 results for September 8, 1993: (a) peak ozone concentration for S2; (b) Peak ozone concentration for S3 at the S2 peak time; (c) ozone concentration difference (S3-S2) at the S2 peak hour; (d) and ozone concentration difference (S3-S2) at hour of maximum difference.	3-6
3-7. S3 results for September 10, 1993: (a) peak ozone concentration for S2; (b) peak ozone concentration for S3 at the S2 peak time; (c) ozone concentration difference (S3-S2) at the S2 peak hour; (d) and ozone concentration difference (S3-S2) at hour of maximum difference.	3-7

LIST OF FIGURES (Continued)

<u>Figure</u>	<u>Page</u>
3-8. S4 results for September 8, 1993: (a) peak ozone concentration for base; (b) peak ozone concentration for sensitivity at base peak time; (c) ozone concentration difference (sensitivity-base) at peak hour for base; and (d) ozone concentration difference (sensitivity-base) at hour of maximum difference.....	3-8
3-9. S4 results for September 10, 1993: (a) peak ozone concentration for base; (b) peak ozone concentration for sensitivity at base peak time; (c) ozone concentration difference (sensitivity-base) at peak hour for base; and(d) ozone concentration difference (sensitivity-base) at hour of maximum difference.....	3-9
3-10. S5 results for September 8, 1993: (a) peak ozone concentration for base; (b) peak ozone concentration for sensitivity at base peak time; (c) ozone concentration difference (sensitivity-base) at peak hour for base; and (d) ozone concentration difference (sensitivity-base) at hour of maximum difference.....	3-10
3-11. S5 results for September 9, 1993: (a) peak ozone concentration for base; (b) peak ozone concentration for sensitivity at base peak time; (c) ozone concentration difference (sensitivity-base) at peak hour for base; and (d) ozone concentration difference (sensitivity-base) at hour of maximum difference.....	3-11
3-12. S5 results for September 10, 1993: (a) peak ozone concentration for base; (b) peak ozone concentration for sensitivity at base peak time; (c) ozone concentration difference (sensitivity-base) at peak hour for base; and (d) ozone concentration difference (sensitivity-base) at hour of maximum difference.....	3-12
3-13. S6 results for September 8, 1993: (a) peak ozone concentration for base; (b) peak ozone concentration for sensitivity at base peak time; (c) ozone concentration difference (sensitivity-base) at peak hour for base; and (d) ozone concentration difference (sensitivity-base) at hour of maximum difference.....	3-13
3-14. S6 results for September 10, 1993: (a) peak ozone concentration for base; (b) peak ozone concentration for sensitivity at base peak time; (c) ozone concentration difference (sensitivity-base) at peak hour for base; and (d) ozone concentration difference (sensitivity-base) at hour of maximum difference.....	3-14
3-15. S7 results for September 8, 1993: (a) peak ozone concentration for base; (b) peak ozone concentration for sensitivity at base peak time; (c) ozone concentration difference (sensitivity-base) at peak hour for base; and (d) ozone concentration difference (sensitivity-base) at hour of maximum difference.....	3-15
3-16. S7 results for September 10, 1993: (a) peak ozone concentration for base; (b) peak ozone concentration for sensitivity at base peak time; (c) ozone concentration difference (sensitivity-base) at peak hour for base; and (d) ozone concentration difference (sensitivity-base) at hour of maximum difference.....	3-16

LIST OF FIGURES (Continued)

<u>Figure</u>	<u>Page</u>
3-17. S8 results for September 8, 1993: (a) peak ozone concentration for S5; (b) peak ozone concentration for Sensitivity 8 at the S5 peak time; (c) ozone concentration difference (S8-S5) at the S5 peak hour; and (d) ozone concentration difference (S8-S5) at hour of maximum difference.	3-17
3-18. S8 results for September 9, 1993: (a) peak ozone concentration for S5; (b) peak ozone concentration for S8 at the S5 peak time; (c) ozone concentration difference (S8-S5) at the S5 peak hour; and (d) ozone concentration difference (S8-S5) at hour of maximum difference.	3-18
3-19. S8 results for September 10, 1993: (a) peak ozone concentration for S5; (b) peak ozone concentration for S8 at the S5 peak time; (c) ozone concentration difference (S8-S5) at the S5 peak hour; and (d) ozone concentration difference (S8-S5) at hour of maximum difference.	3-19
3-20. S9 results for September 8, 1993: (a) peak ozone concentration for base; (b) peak ozone concentration for sensitivity at base peak time; (c) ozone concentration difference (sensitivity-base) at peak hour for base; and (d) ozone concentration difference (sensitivity-base) at hour of maximum difference.	3-20
3-21. S9 results for September 10, 1993: (a) peak ozone concentration for base; (b) peak ozone concentration for sensitivity at base peak time; (c) ozone concentration difference (sensitivity-base) at peak hour for base; and (d) ozone concentration difference (sensitivity-base) at hour of maximum difference.	3-21
3-22. S10 results for September 8, 1993: (a) peak ozone concentration for base; (b) peak ozone concentration for sensitivity at base peak time; (c) ozone concentration difference (sensitivity-base) at peak hour for base; and (d) ozone concentration difference (sensitivity-base) at hour of maximum difference.	3-22
3-23. S10 results for September 10, 1993: (a) peak ozone concentration for base; (b) peak ozone concentration for sensitivity at base peak time; (c) ozone concentration difference (sensitivity-base) at peak hour for base; and (d) ozone concentration difference (sensitivity-base) at hour of maximum difference.	3-23
3-24. S11 results for September 8, 1993: (a) peak ozone concentration for base; (b) peak ozone concentration for sensitivity at base peak time; (c) ozone concentration difference (sensitivity-base) at peak hour for base; and (d) ozone concentration difference (sensitivity-base) at hour of maximum difference.	3-24
3-25. S11 results for September 10, 1993: (a) peak ozone concentration for base; (b) peak ozone concentration for sensitivity at base peak time; (c) ozone concentration difference (sensitivity-base) at peak hour for base; and (d) ozone concentration difference (sensitivity-base) at hour of maximum difference.	3-25

LIST OF FIGURES (Concluded)

<u>Figure</u>	<u>Page</u>
3-26. Cloud fraction on September 8, 1993	3-26
3-27. Cloud fraction on September 9, 1993 at 1200 CST	3-27
3-28. Cloud fraction on September 10, 1993 at 1200 CST	3-27
3-29. Cloud sensitivity ozone difference (sensitivity – base) at 1300 CST on September 9, 1993	3-28
3-30. Cloud sensitivity ozone difference (sensitivity – base) at 1600 CST on September 9, 1993	3-29
3-31. Time series of grid cell predicted ozone at selected monitoring sites for the base case and the cloud sensitivity simulation.....	3-30
3-32. Four largest spike intensities calculated in the Houston area domain.	3-34
3-33. S12 upset from 1000 to 1200 CST at Chocolate Bayou on September 10, 1993 showing ozone differences from the base case at (a) 1100 CST, (b) 1200 CST, (c) 1400 CST, and (d) 1600 CST.....	3-37
4-1. The spike intensity can be reduced when the minimum occurs during the nighttime due to titration.	4-3
4-2. The greatest negative change occurs before the maximum positive change in this case and is not necessarily representative of a transient high ozone event.....	4-4

LIST OF TABLES

<u>Table</u>	<u>Page</u>
2-1. Description of 12 sensitivity runs.	2-1
2-2. Assignment of image estimated cloud fraction to simulation hour.	2-4
3-1. SAS moments and quantiles for the spike intensity for the base-case 16-km grid.	3-31
3-2. SAS moments and quantiles for the spike intensity for the base-case 4-km grid.	3-31
3-3. SAS Moments and Quantiles for the spike intensity for S5 (clouds) 16-km grid.	3-32
3-4. SAS Moments and Quantiles for the spike intensity for S5 (clouds) 4-km grid.	3-32
3-6. SAS Moments and Quantiles for the spike intensity for S7 (upset) 4-km grid.	3-33
3-7. SAS moments and quantiles for the spike intensity for the base-case 16-km grid for September 8 and September 10.	3-35
3-8. SAS moments and quantiles for the spike intensity for the base-case 4-km grid for September 8 and September 10.	3-35
3-9. SAS moments and quantiles for the spike intensity for S12 (2-hr upset) 16-km grid for September 8 and September 10.	3-36
3-10. SAS moments and quantiles for the spike intensity for S12 (2-hr upset) 4-km grid for September 8 and September 10.	3-36

1. INTRODUCTION

The Comprehensive Air Quality Model with extensions (CAMx) was previously applied in the Houston-Galveston Area (HGA) for an ozone episode during the September 6-11, 1993 period. In earlier analyses of CAMx modeling for the HGA, several questions were raised concerning the causes of high simulated ozone in the area and the response of CAMx to emission reductions. More recently, preliminary results from the TexAQS2000 study raised questions about emission inventories from industrial sources and the role of upset emission conditions in the rapid formation of ozone.

The goals of this work were to isolate the cause of an area of ozone overprediction in the original modeling, assess the impact of cloud cover on CAMx ozone predictions, and determine if rapid ozone production events can be simulated with CAMx.

It was originally planned that seven CAMx sensitivity simulations would be performed and the following types of simulations were suggested:

- Emission sensitivity simulations to isolate the source categories and locations that contribute to overpredictions of ozone on September 8
- A simulation without NO_x emissions from the W.A. Parish power plant in Fort Bend County to assess the plants impact on peak ozone concentrations
- Simulations with alternative Plume-in-Grid treatments to investigate their effect on ozone formation downwind of the W.A. Parish power plant
- A simulation using cloud fields in CAMx to asses the impact of cloud cover on photolysis and resulting model performance
- An emission mass sensitivity simulation approximating upset conditions at a major chemical plant to assess whether CAMx can simulate upset-related rapid ozone formation events
- An emission speciation sensitivity simulation to test possible limitations of the CB-IV chemical mechanism to represent fast-reacting species in rapid ozone formation events
- Two or more sensitivity simulations where meteorological inputs (winds and vertical diffusion) to assess the impact of meteorology on rapid ozone production events

However, as the simulations proceeded, certain issues were resolved and the list of simulations was modified based on results and new questions that arose. A total of 12 sensitivity simulations were finally performed. This report describes those simulations and the results obtained. The basic description of the simulations and the methods used to carry them out are provided in Section 2. Section 3 presents the results of the simulations. Section 4 provides a discussion of the sensitivity simulation results in the context of issues being investigated. Section 5 presents the study's conclusions and provides recommendations for future modeling efforts in the HGA. References are provided in Section 6.

2. METHODOLOGY

2.1 SENSITIVITY SIMULATIONS

In order to investigate the abilities and limitations of CAMx in assessing HGA air quality and control strategies, STI performed 12 sensitivity simulations. These sensitivity simulations were used to address the specific concerns listed in Section 1 by isolating and adjusting the given input parameters of the base case model (the original model). The sensitivity modeling was a dynamic process with results of early cases determining how to adjust later cases. The 12 sensitivity runs are summarized in **Table 2-1**.

Table 2-1. Description of 12 sensitivity runs.

Sensitivity Case	Description
Sensitivity 1 (S1)	Zero NO _x emissions from W.A. Parish power plant
Sensitivity 2 (S2)	Base Case with -50% NO _x reduction
Sensitivity 3 (S3)	Case S1 with -50% NO _x reduction
Sensitivity 4 (S4)	Zero Ship Channel elevated NO _x
Sensitivity 5 (S5)	Cloud fields on September 8-10, 1993
Sensitivity 6 (S6)	Zero low level NO _x in Houston core
Sensitivity 7 (S7)	10*ETH and 10*OLE at Texas City and Chocolate Bayou
Sensitivity 8 (S8)	Cloud (S5) with 50% NO _x reduction
Sensitivity 9 (S9)	3*ETH and 3*OLE in Ship Channel
Sensitivity 10 (S10)	S7 with 25% reduction in wind speed
Sensitivity 11 (S11)	S7 with 25% reduction in K _v
Sensitivity 12 (S12)	10*ETH; 10*OLE at Chocolate Bayou from 1000 to 1200 CST on September 8 and September 10

All simulations were made using CAMx Version 2.03 for the SuperCOAST domain as shown in Figure 2-1. The SuperCOAST domain consists of a coarse grid with 16-km horizontal grid spacing and a nested fine grid with 4-km grid spacing. For all simulations, both grids were used. However, the analyses performed for this report focus on the fine grid results.

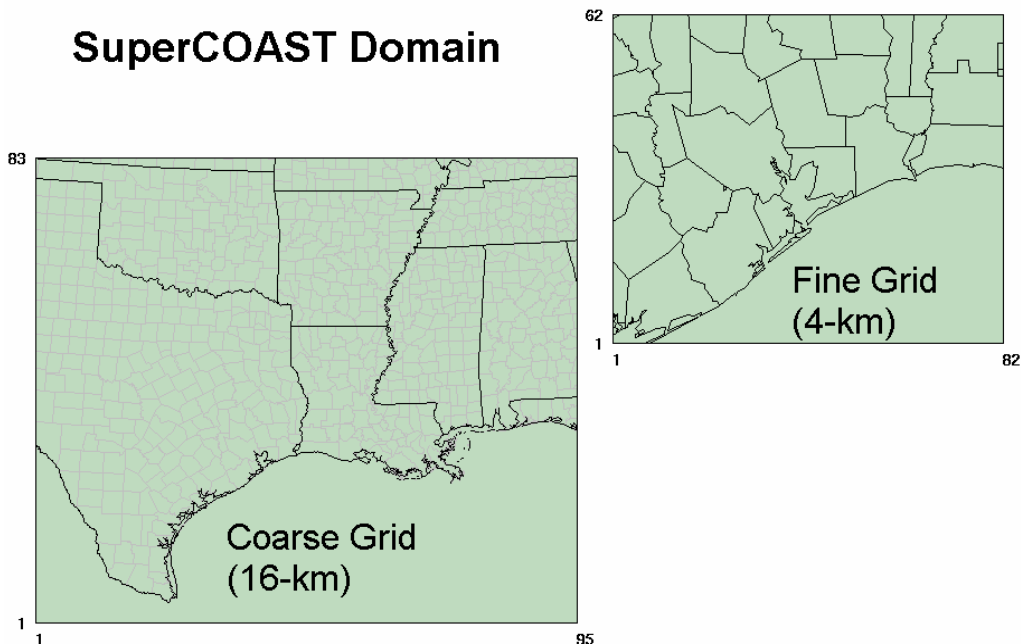


Figure 2-1. Coverage of the SuperCOAST domain.

2.1.1 Sensitivity 1 – Zero NO_x at W.A. Parish Power Plant

In Sensitivity 1 (S1) the NO_x emissions from the W.A. Parish power plant in Fort Bend County were set to zero. This power plant, southwest of the city of Houston, is a large NO_x point source. Because of the plant's proximity to the area of peak simulated ozone, this plant was suspected to significantly affect simulated ozone. The plant was removed by setting the NO and NO₂ emissions for the cell containing the power plant to zero in the input point source emissions file. A program was written to make this modification to the input file; and the file was checked visually using the Package for Analysis and Visualization of Environmental data (PAVE). PAVE is an application used to visualize CAMx input and output files (Thorpe, 1996). This check was performed for all the sensitivity cases.

2.1.2 Sensitivity 2 – Domain-Wide 50% NO_x Reduction

Sensitivity 2 (S2) involved reducing the domain-wide NO_x emissions by 50%. FORTRAN programs were written to modify both the point source and area source input file emissions by 50%. This simulation provided a benchmark to compare later sensitivity simulations involving NO_x reductions.

2.1.3 Sensitivity 3 – 50% NO_x Reduction without W.A. Parish Power Plant

In Sensitivity 3 (S3) domain-wide NO_x were reduced by 50% from the S1 emissions. The FORTRAN programs written for S2 were used on the input emissions for S1 to create the input files for area and point sources. This simulation was performed to assess the W.A. Parish power plant's affect on the modeling system's response to reductions of NO_x emission

2.1.4 Sensitivity 4 – Zero NO_x in the Houston Ship Channel

Sensitivity 4 (S4) involved setting elevated NO_x emissions in the Houston Ship Channel to zero. The Ship Channel is an extremely large industrial source east of the city. Removing the Ship Channel NO_x emissions allowed their impact on the modeled peak ozone to be evaluated. These emissions were removed by identifying elevated point sources in the vicinity of the Ship Channel and setting their NO and NO₂ emissions to zero.

2.1.5 Sensitivity 5 – Cloud Cover

Sensitivity 5 (S5) involved introducing cloud fields for three days of the simulation period to assess the impact of cloud cover on ozone production. CAMx Cloud Cover input files were created for September 8, 9, and 10, 1993, for sensitivity simulations of the September 1993 HGA ozone episode. The input files are UAM-V type files containing cloud fraction and liquid water content. The Cloud Cover input file specifies the cloud fraction obscuring the sky above the grid cell and the liquid water content for the grid cell. Satellite imagery was used to specify the cloud fraction. GOES 7 weather satellite sector imagery was available six times a day. These images were used to calculate the fraction of cloud versus clear sky for each 16-km square coarse grid cell. Liquid water content was assumed to be a typical value for cumulus clouds in continental polluted air. However, CAMx does not currently use the liquid water content in any calculation.

The satellite imagery is 1-km resolution visible imagery from GOES 7. The images covered approximately the area bounded by 25 to 37 degrees north latitude and 86 to 102 degrees west longitude. This area only covers part of the 16-km coarse grid domain. Cloud fraction for areas outside the region of the satellite images was set to zero, clear sky. Imagery was available six times a day during daylight hours only. From sunset until sunrise the cloud fraction was set to zero, clear sky. The satellite images were labeled in Central Daylight Time (CDT). Times were adjusted to Central Standard Time (CST). Sunrise for this period in Houston, Texas, was 0603 CST and sunset was 1834 CST. Cloud fractions estimated from the imagery were assigned to time periods as shown in **Table 2-2**.

Table 2-2. Assignment of image estimated cloud fraction to simulation hour.

Simulation Hour	Image Time CST
0000-0500	Constant 0.0 Cloud Fraction
0600-0700	0731 Image
0800-0900	0831 Image
1000-1100	1031 Image
1200-1300	1231 Image
1400-1500	1431 Image
1600-1800	1631 Image
1900-2300	Constant 0.0 Cloud Fraction

The satellite images are in JPEG format. Each image was 1265 pixels left-right and 990 pixels top-bottom. The images are gray-scale with 8 bits of data per pixel. The images were processed with the computer program, ImageJ (Rasband, 2000). ImageJ is a public domain Java image processing program distributed by the National Institute for Mental Health. Geo-location data for the satellite images were not available. The pixels were located within the coarse grid with transformation equations relating pixel number to the coarse grid domain UTM coordinates. The transformation equations were created by selecting 22 control points at the intersections of latitude-longitude grid lines. The pixel locations I (1-1265) and J (1-990) of the latitude-longitude grid intersections were read with ImageJ. Two equations were created, one for the UTM Easting and one for the UTM Northing. The transformation equations are:

$$\text{UTM Northing} = a1 + b1*I + c1*J + d1*I*I + e1*J*J$$

$$\text{UTM Easting} = a2 + b2*I + c2*J + d2*I*I + e2*J*J .$$

The coefficients in these equations were determined using multiple regression where the pixel locations I and J are the independent variables and the UTM Northing and Easting for the latitude-longitude grid line intersections are the dependent variables. The standard error for the Northing equation is 492 m, and 533 m for the Easting equation. Geo-location errors for any given pixel may be larger but should be on the order of 1 km or less. The transformation equations were developed using only the September 8, 1993, 0831 CDT, image. The images all appear to display the same region; however, there may be small displacements between images that could contribute to increased error in geo-locating the pixels.

The images were subjected to threshold processing in ImageJ. This process created a black-white image from the gray-scale satellite image. The process was quite successful in identifying the clouds in the images. **Figure 2-2** is a JPEG satellite image and **Figure 2-3** is the image created by the threshold process. Artifacts of latitude-longitude grid lines and annotations still appear in the images. These artifacts were removed manually using image tools in Adobe

PhotoDeluxe, a commercial software program. The artifacts were erased and the areas made either black or white depending on whether clouds were present. **Figure 2-4** shows the image after removal of the artifacts. The image created after removal of the artifacts was saved as a delimited data file with 1265 columns and 990 rows with values of 0 to 255 for each pixel. Zero represents completely black and 255 completely white.

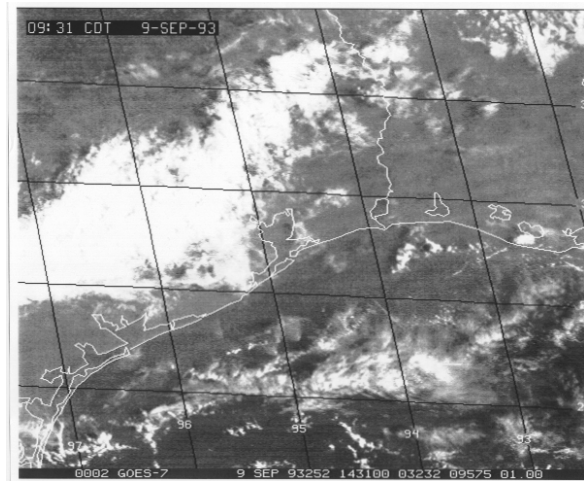


Figure 2-2. Initial satellite image.

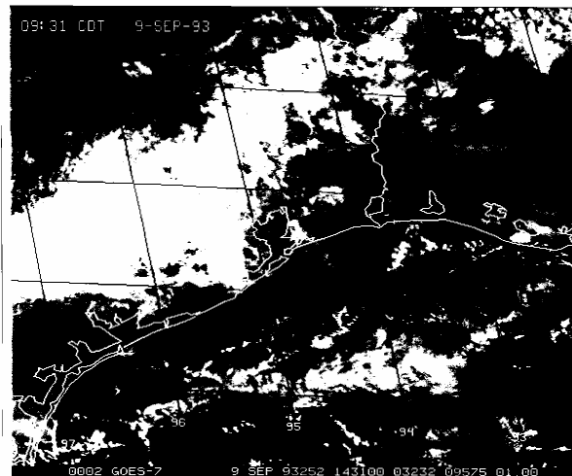


Figure 2-3. Satellite image after threshold processing.

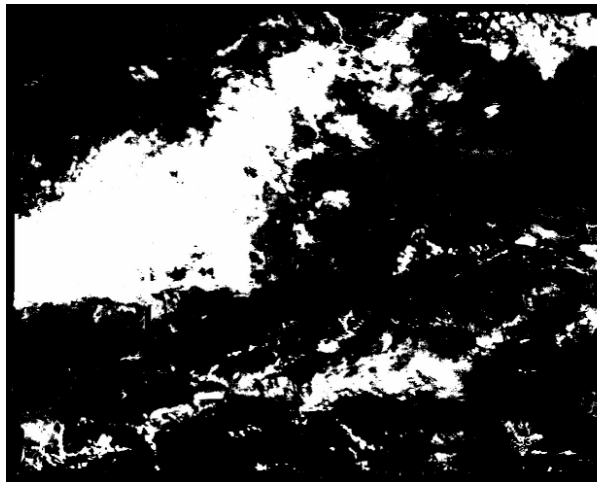


Figure 2-4. Final satellite image after artifact removal.

The cloud fraction for each 16km square grid cell in the CAMx coarse grid was calculated from the data file created by the procedure described above. The number of pixels located within each 16km grid cell was counted. The cloud fraction is the number of cloud pixels (value ≥ 200) divided by the total number of pixels within the grid cell.

There was no information available to identify the cloud types or the height and depth of the clouds. The cloud fraction was assigned to all vertical layers (8 total) in the CAMx domain. This is the same as assuming that the clouds extend from their base to above the model domain.

A non-zero value for liquid water content was used for those grid cells with a cloud fraction 0.1 or greater and the vertical layer was at cloud base or above. Liquid water content was set to zero elsewhere. Cloud base was assumed to be layer 6 for September 8, and layer 5 for September 9 and 10. These layers for cloud base were estimated by examining the CAMx water vapor input files. There was an indication of clouds in layers 6 and 7 in the water vapor on September 8. On September 9 there was an indication of clouds in layers 5 and 6. On September 10 there was an indication of clouds in layers 5, 6, and 7. Liquid water content was specified for layers 6, 7, and 8 on September 8 and layers 5, 6, 7, and 8 on September 9 and 10. This assumes that the clouds extend from the base to above the model domain. The value for liquid water content was set to 0.3 g/m^3 . This value is typical of a cumulus cloud in polluted continental air (Hess et al., 1998).

Cloud fraction and liquid water content were written to a binary UAM-V type Cloud Cover input file for input into CAMx. A separate file for 0000 to 2300 CST was created for each day—September 8, 9, and 10, 1993.

2.1.6 Sensitivity 6 – Zero NO_x in Central Houston

Sensitivity 6 (S6) involved setting NO_x emissions in central Houston to zero for low-level sources (primarily mobile source emissions). Mobile source emissions are a large NO_x

source in the city and can affect Houston air quality significantly. The purpose of the simulation was to assess the contribution of central Houston NO_x emissions to peak ozone in the Houston area. These emissions were removed by setting the NO and NO₂ to zero in the area source input files for cells in central Houston.

2.1.7 Sensitivity 7 – Continuous Emission Upset

Sensitivity 7 (S7) was designed to simulate a continuous chemical upset arising from non-standard operation. In this case, the emissions of ethylene (ethene) and propylene (propene) from chemical plants in Chocolate Bayou and Texas City were increased. The emissions for these chemical species were increased 10 times. In a NO_x-rich environment, these hydrocarbons can be a limiting factor in ozone formation; and with greater hydrocarbon release, ultimately one would expect higher ozone concentrations. The chemical emissions were increased by adjusting ETH (ethylene) and OLE (the Carbon Bond IV species representing propylene) in the CAMx emissions inputs by a factor of 10 in the cells representing Chocolate Bayou and Texas City with a previously developed program. The locations of these cells are shown in **Figure 2-5**.

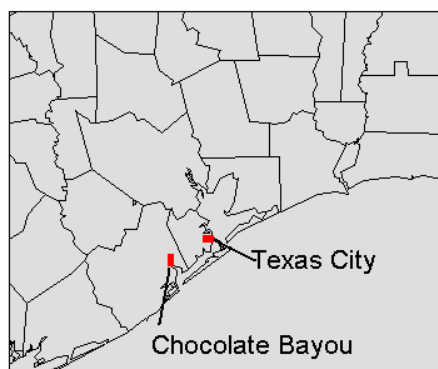


Figure 2-5. Location of grid cells representing Chocolate Bayou and Texas City.

2.1.8 Sensitivity 8 – 50% NO_x Reduction with Cloud Cover

Sensitivity 8 (S8) involved introducing cloud cover as in S5 with a 50% reduction in NO_x emissions. The purpose of this simulation was to evaluate the effect of cloud cover on the model's response to NO_x emission reductions. The simulation used S5 cloud files and S2 emissions files as inputs.

2.1.9 Sensitivity 9 – Enhanced Ship Channel Emissions of Ethene and Propene

Sensitivity 9 (S9) was designed to assess the impacts of potential underestimates of ethylene (ethene) and propylene (propene) from the Ship Channel as suggested by recent measurement studies. The emissions for these chemical species were increased 3 times, a number that may be realistic if emissions are under-reported in this area. In a NO_x-rich environment, these hydrocarbons can be a limiting factor in ozone formation; and with greater

hydrocarbon release, ultimately one would expect higher ozone concentrations. The chemical emissions were increased by adjusting ETH (Carbon Bond IV species for ethylene) and OLE (Carbon Bond IV species representing propylene) in the CAMx emissions inputs by a factor of 3 in the cells representing the Ship Channel with a previously developed routine.

2.1.10 Sensitivity 10 and 11 – Reduced Transport and Diffusion

Sensitivities 10 and 11 (S10 and S11) were designed to assess the impact of meteorology on rapid ozone formation in CAMx. Both simulations used emissions from S7 that simulate a continuous enhancement of ethene and propene emissions at Texas City and Chocolate Bayou. However, in S10 the winds were decreased by 25%, and the vertical diffusion coefficient, K_v , was decreased by 25 % in S11. FORTRAN programs were written to modify both the wind field and the vertical diffusion input files. In the case of vertical diffusion, the CAMx model limits the values of K_v when the model post-processes the input file; therefore, it was necessary to pre-process the input file in this same way and then apply the 25% reduction. Routines were written to apply these changes to the entire domain.

2.1.11 Sensitivity 12 – Limited Duration Emissions Upset

Sensitivity 12 (S12) investigated the impact of a simulated emissions upset limited to periods from 1000 to 1200 CST on September 8 and 10 at Chocolate Bayou. Ethene (ETH in CAMx) and propene (OLE in CAMx) were increased 10 times during these periods. The purpose of this simulation was to compare the impact from short duration emission upsets with those from continuous increases simulated in S7.

2.2 SPIKE INTENSITY CALCULATION

The distribution of spike intensities within the model domains was investigated for some of the sensitivity simulations using a definition suggested by Jolly (2001):

$$\text{Spike_Intensity} = (\Delta \text{min} + \Delta \text{max})/\text{length}$$

where Δmax is the greatest 1-hr increase in ozone during the day, Δmin is the greatest 1-hr decrease in ozone during the day, and length is time in hours between the occurrence of Δmin and Δmax . A FORTRAN program was written to calculate this parameter for each cell in the Houston area, as shown in **Figure 2-6**, for each day of the simulation. Statistics to describe the distribution of spike intensities were calculated over the Houston area using the SAS UNIVARIATE procedure (SAS, 2000).

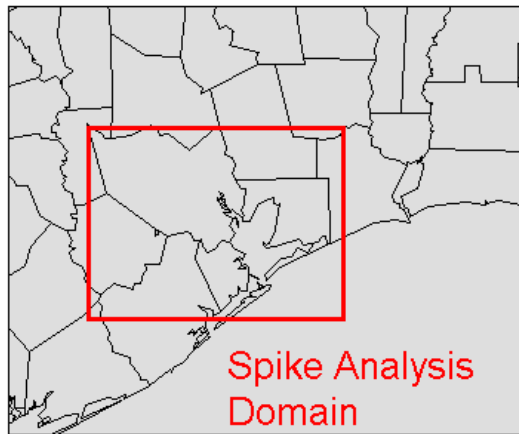


Figure 2-6. Spike analysis region.

3. RESULTS

3.1 SENSITIVITY SIMULATIONS

In this section, a summary of the sensitivity results is provided for ozone concentrations. In addition, figures for the peak ozone hours and specific days for the simulation are shown in comparison with a base case. The figures for all these cases are shown for September 8 and 10. Cloud cover sensitivity runs for September 9 are provided as well. Results for most of the sensitivity simulations are shown in **Figure 3-1**. The base case ozone concentrations for the peak hour are displayed at the upper left with the ozone concentrations for the sensitivity case, at the same hour, at the upper right. The bottom left panel shows the difference in ozone concentrations (sensitivity – base) at the same peak hour. The lower right panel provides the difference in ozone concentrations at the hour of maximum difference. Exceptions to this layout are S3, where S2 is used as the base, and S8, where S5 is taken as the base.

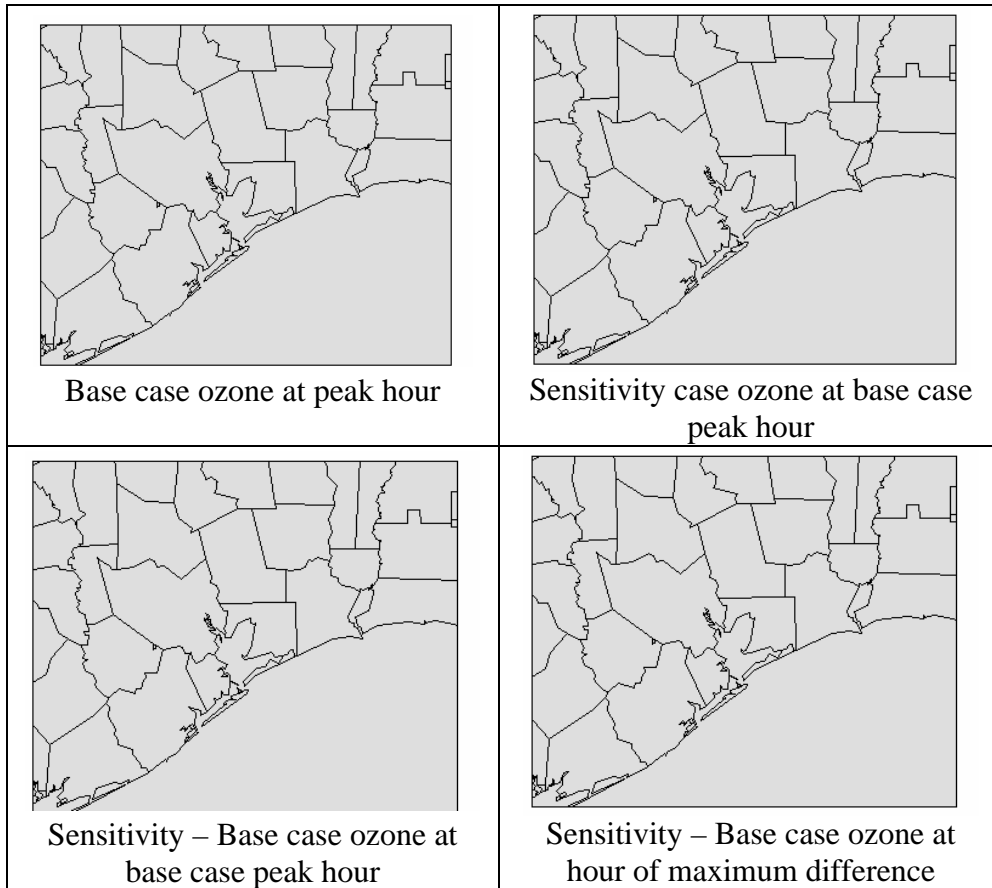


Figure 3-1. Arrangement of sensitivity simulation figures.

In S1 (**Figures 3-2 and 3-3**), the removal of the power plant NO_x emissions has little effect on the Houston area for the days simulated. The peak cell on September 8, 1993 at 1600 CST in the simulation decreased from 187 ppb to 186 ppb, and the largest effect is shown

to be primarily local in nature; higher decreases in ozone concentrations around the power plant are observed. Likewise, the peak cell for September 10, 1993, at 1600 CST remains unchanged at 172 ppb. Again, the largest effects are seen near the power plant location. Transport of the power plant plume during this simulation appears to be away from the city and a major reason there is not a marked effect.

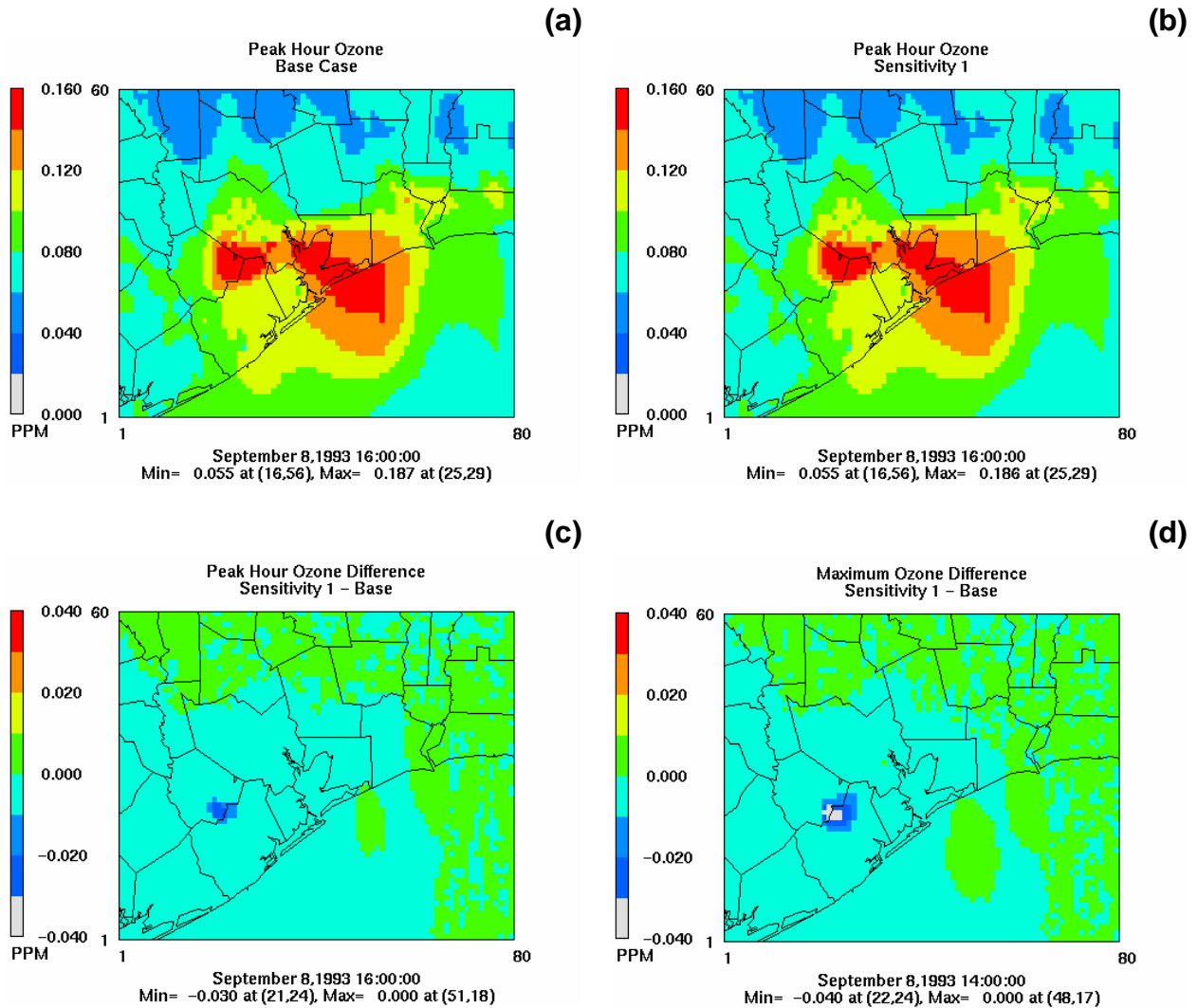


Figure 3-2. S1 results for September 8, 1993: (a) peak ozone concentration for base; (b) peak ozone concentration for sensitivity at base; (c) peak time ozone concentration difference (sensitivity-base) at peak hour for base; (d) and ozone concentration difference (sensitivity-base) at hour of maximum difference.

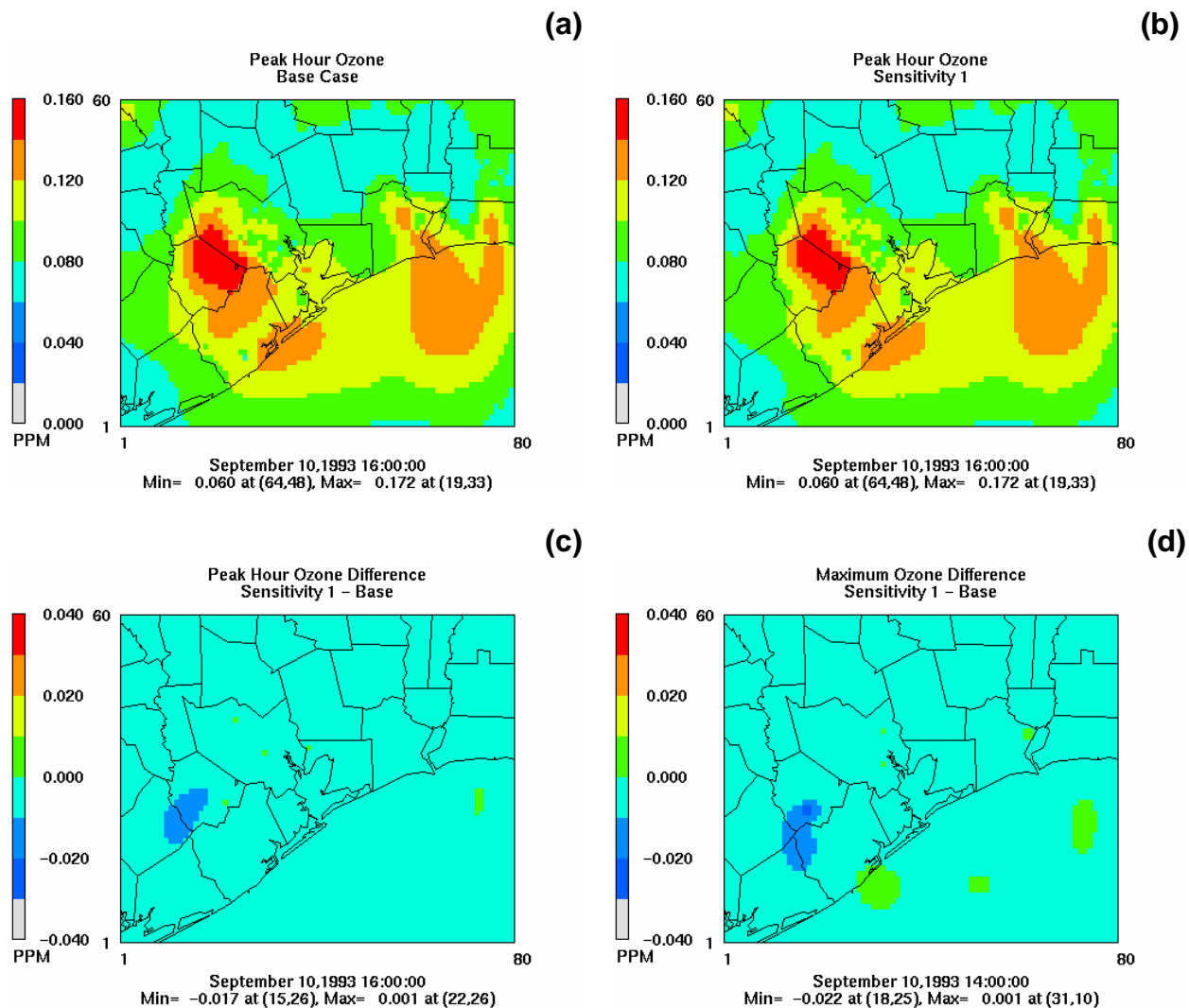


Figure 3-3. S1 results for September 10, 1993: (a) peak ozone concentration for base; (b) peak ozone concentration for sensitivity at base peak time; (c) ozone concentration difference (sensitivity-base) at peak hour for base; and (d) ozone concentration difference (sensitivity-base) at hour of maximum difference.

In S2 (**Figures 3-4 and 3-5**), the reduction of NO_x emissions by 50% has significant effect on the ozone concentrations in two ways: extent of high ozone and peak cell concentration. The peak cell on September 8 drops from 187 ppb to 160 ppb. Likewise the extent of cells over 120 ppb is significantly reduced. Likewise, the peak cell for September 10, 1993, drops from 172 ppb to 149 ppb. There are significant increases of ozone in early evening over the base case in the urban area due to less titration by emitted NO_x . The concentration levels, however, are usually low during this diminished titration.

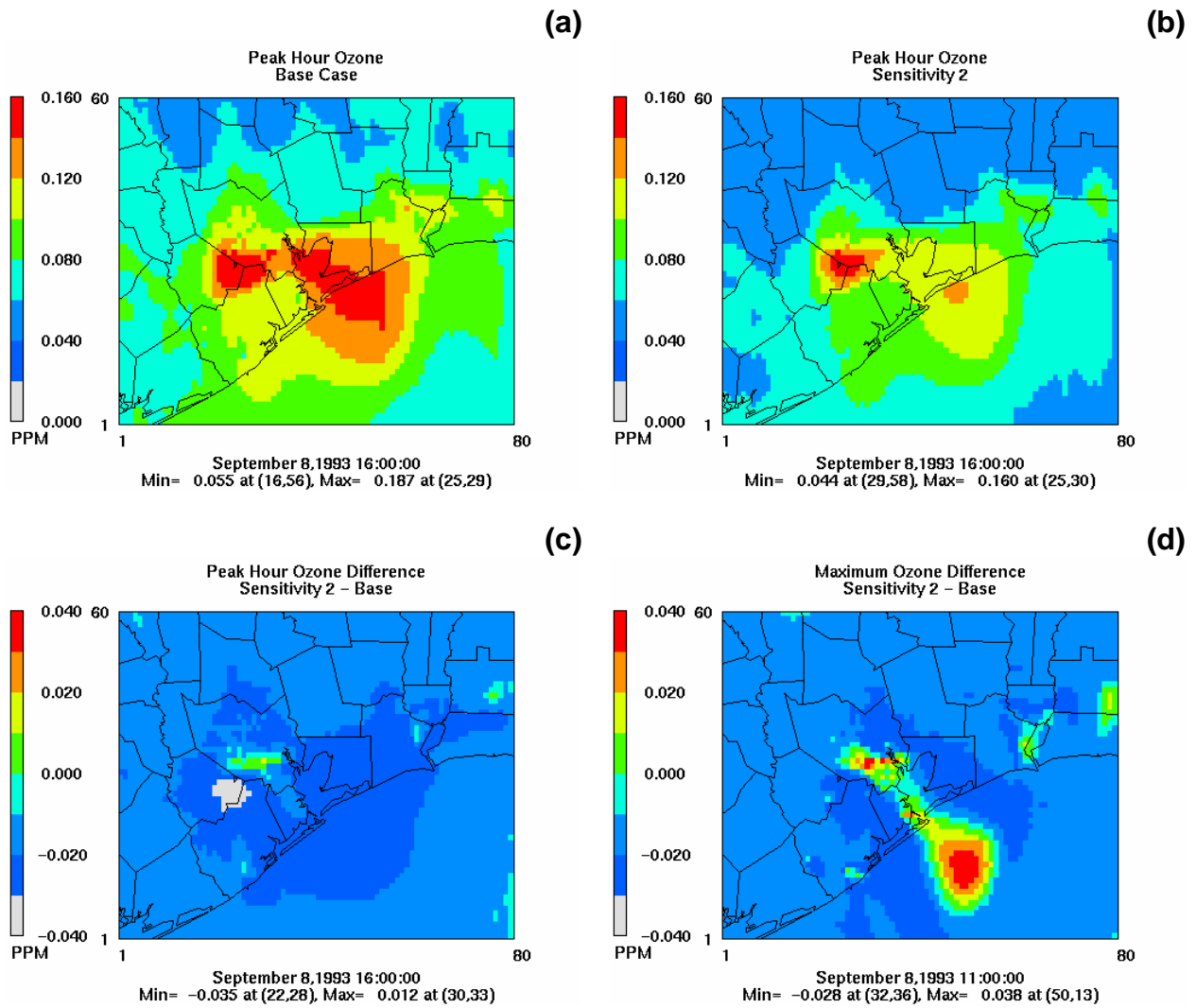


Figure 3-4. S2 results for September 8, 1993: (a) peak ozone concentration for base; (b) peak ozone concentration for sensitivity at base peak time; (c) ozone concentration difference (sensitivity-base) at peak hour for base; and (d) ozone concentration difference (sensitivity-base) at hour of maximum difference.

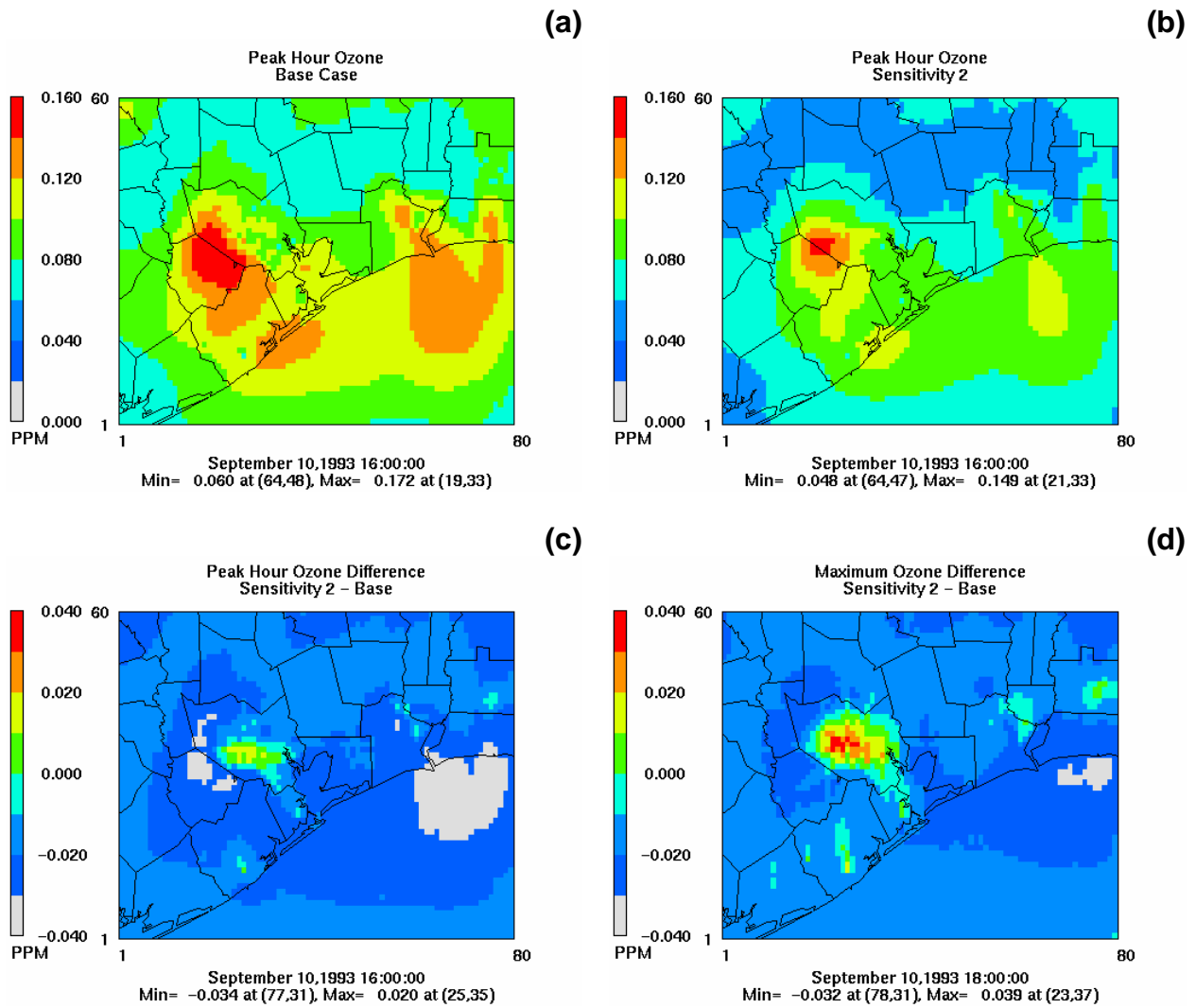


Figure 3-5. S2 results for September 10, 1993: (a) peak ozone concentration for base; (b) peak ozone concentration for sensitivity at base peak time; (c) ozone concentration difference (sensitivity-base) at peak hour for base; and (d) ozone concentration difference (sensitivity-base) at hour of maximum difference.

In S3 (**Figures 3-6 and 3-7**), there is little difference between this case and S2, even though the W.A. Parish Power Plant has been removed. The peak cell for September 8 drops from 160 ppb to 159 ppb; and on September 10, the values change from 149 ppb to 148 ppb. The same conclusions about local effect as in S1 are valid.

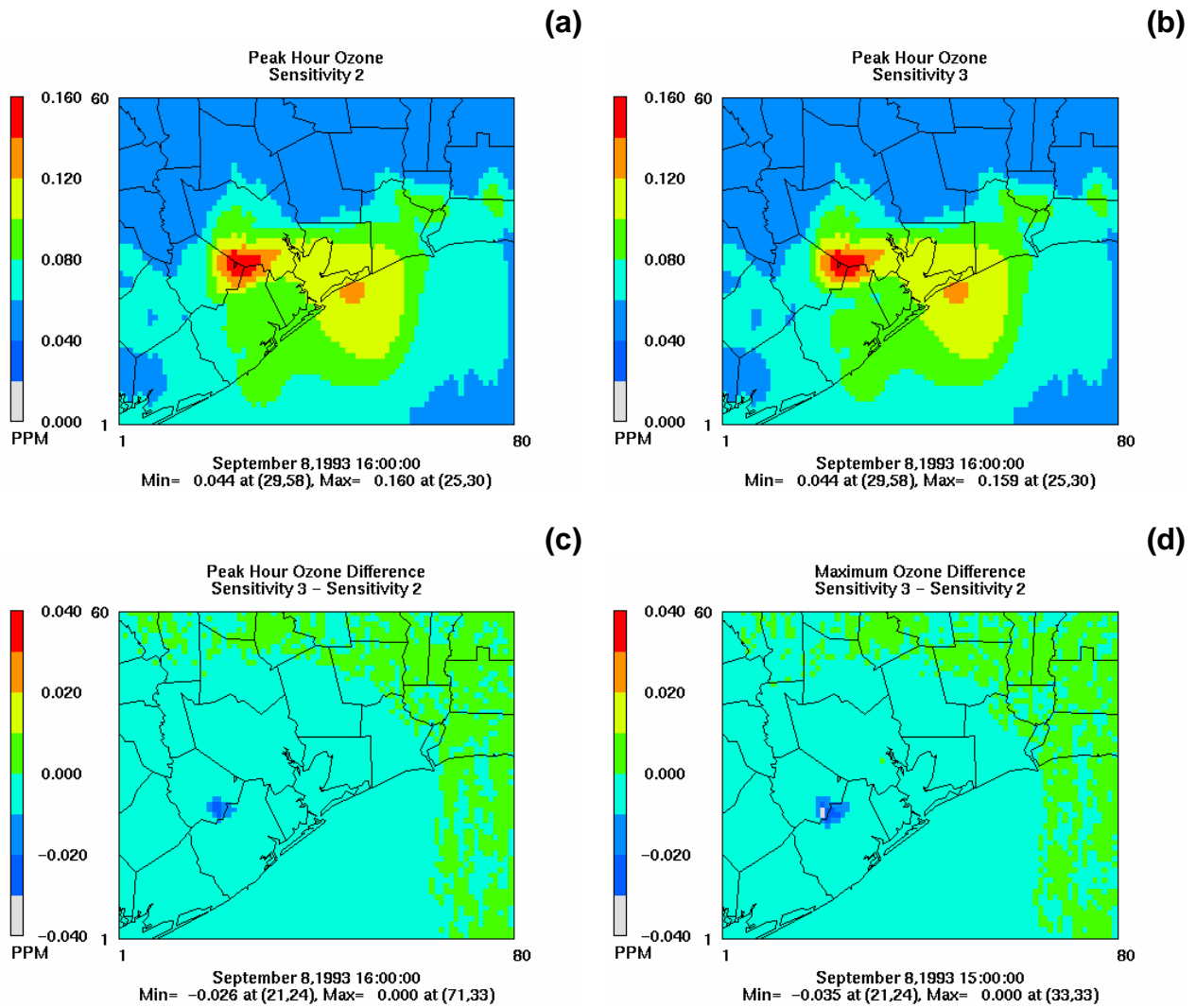


Figure 3-6. S3 results for September 8, 1993: (a) peak ozone concentration for S2; (b) Peak ozone concentration for S3 at the S2 peak time; (c) ozone concentration difference (S3-S2) at the S2 peak hour; (d) and ozone concentration difference (S3-S2) at hour of maximum difference.

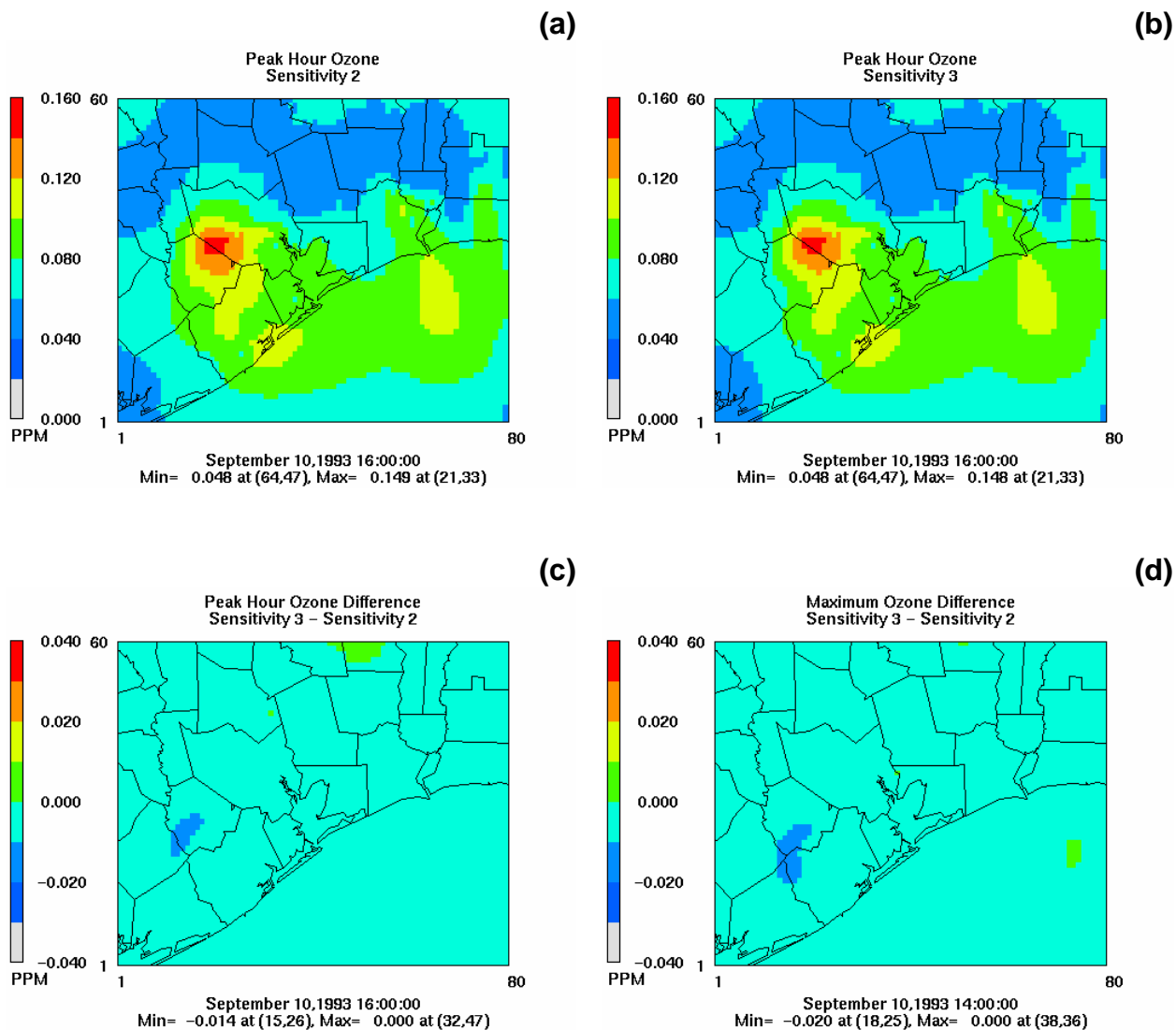


Figure 3-7. S3 results for September 10, 1993: (a) peak ozone concentration for S2; (b) peak ozone concentration for S3 at the S2 peak time; (c) ozone concentration difference (S3-S2) at the S2 peak hour; (d) and ozone concentration difference (S3-S2) at hour of maximum difference.

In S4 (**Figures 3-8 and 3-9**), removing the Ship Channel elevated NO_x emissions has an effect in peak cell values as well as the extent of high concentrations of ozone. The difference between the peak cell for September 8 is 8 ppb, from 187 ppb to 179 ppb, and on September 10, 3 ppb, from 172 ppb to 169 ppb. The extent of the higher concentrations is more dramatically affected as the area of high concentration shrinks, primarily along the Ship Channel. There are significant increases of ozone at nighttime over the Ship Channel in comparison to the base case due to less titration by emitted NO_x at night. The concentration levels, however, rarely exceed 100 ppb during this diminished titration.

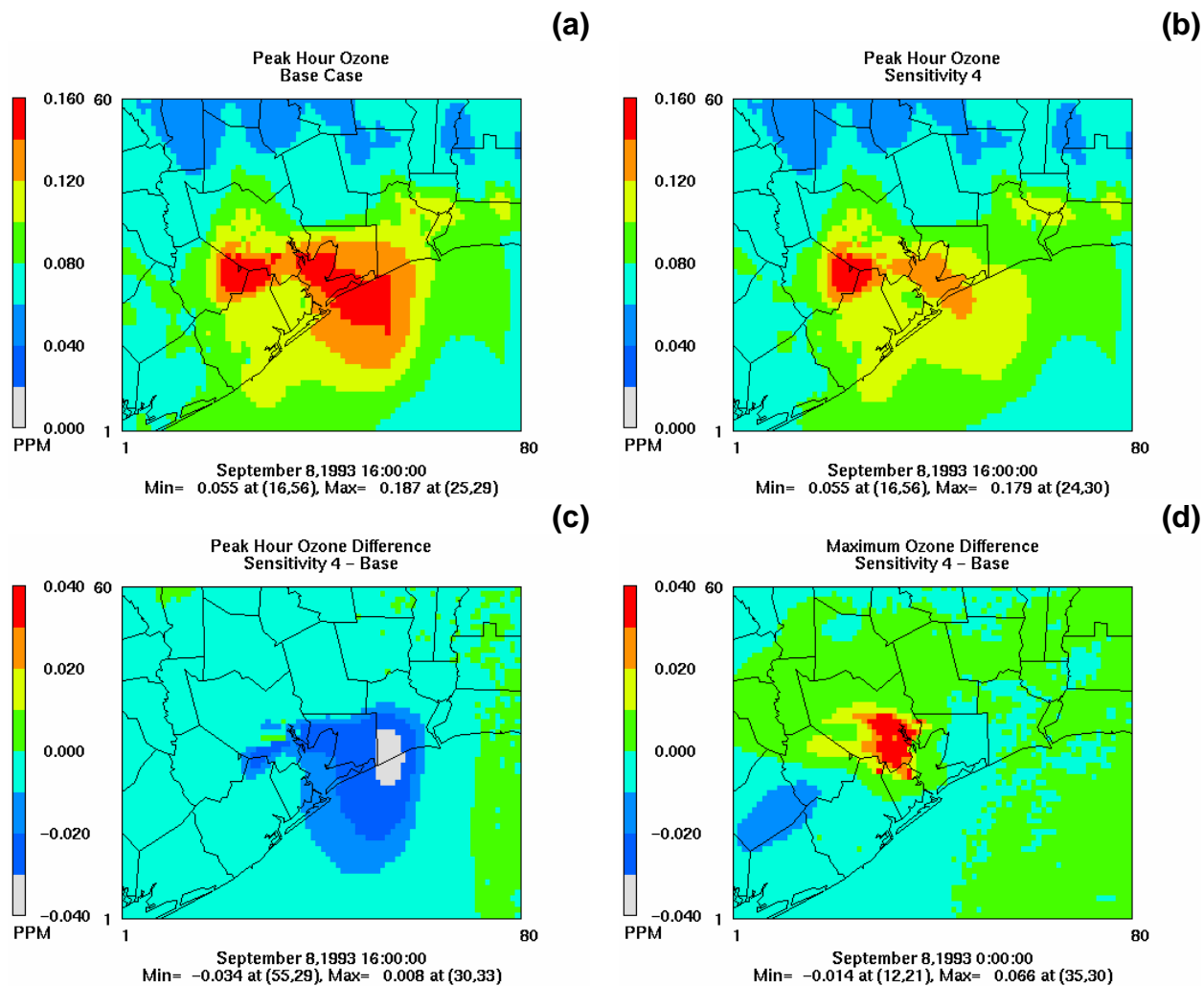


Figure 3-8. S4 results for September 8, 1993: (a) peak ozone concentration for base; (b) peak ozone concentration for sensitivity at base peak time; (c) ozone concentration difference (sensitivity-base) at peak hour for base; and (d) ozone concentration difference (sensitivity-base) at hour of maximum difference.

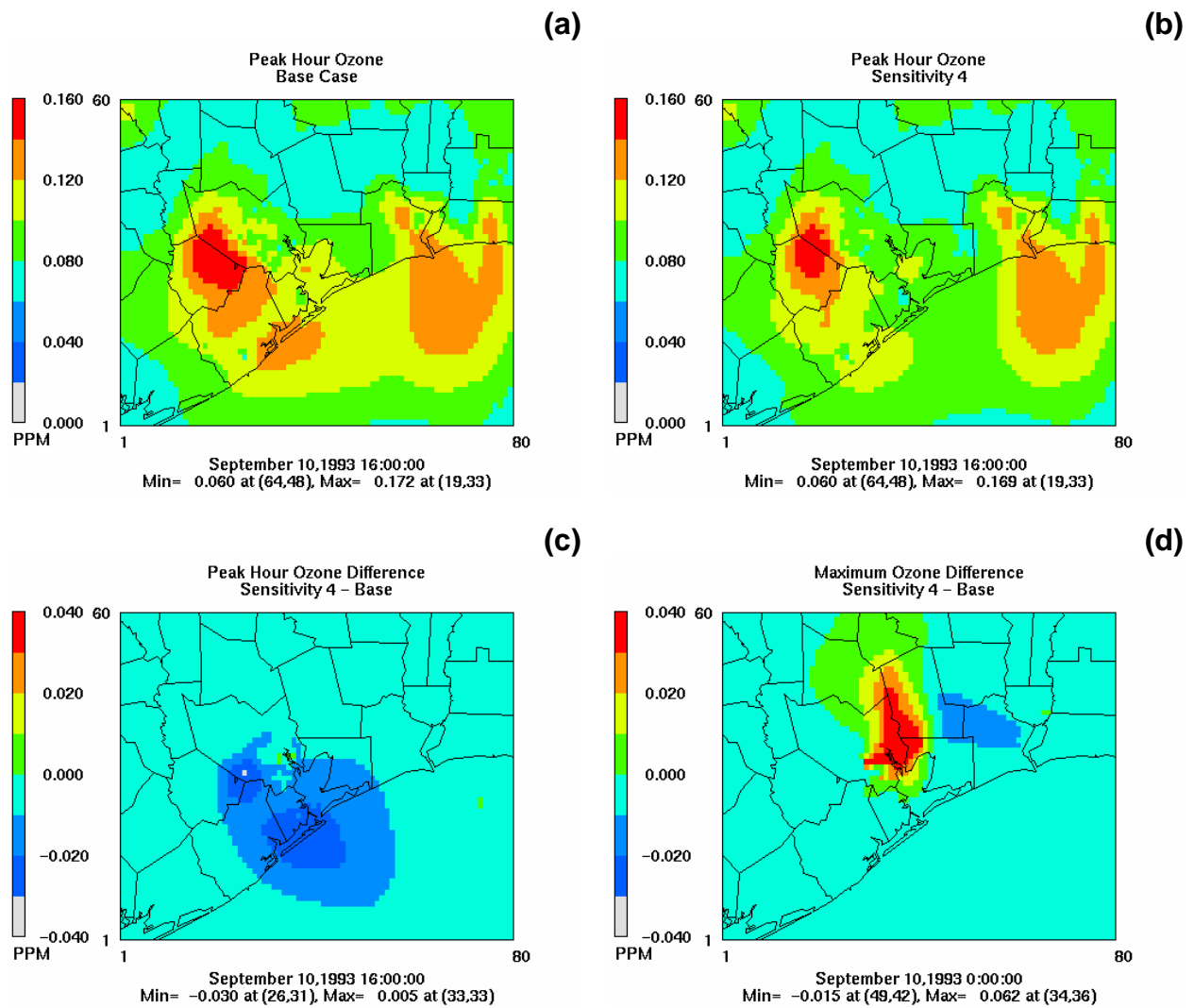


Figure 3-9. S4 results for September 10, 1993: (a) peak ozone concentration for base; (b) peak ozone concentration for sensitivity at base peak time; (c) ozone concentration difference (sensitivity-base) at peak hour for base; and(d) ozone concentration difference (sensitivity-base) at hour of maximum difference.

S5 (Figures 3-10, 3-11, 3-12) shows the effects of introducing a cloud cover. The clouds slightly diminish the peak concentrations with greater effects in non-peak cells. These results are discussed in more detail in Section 3.2 on cloud effects.

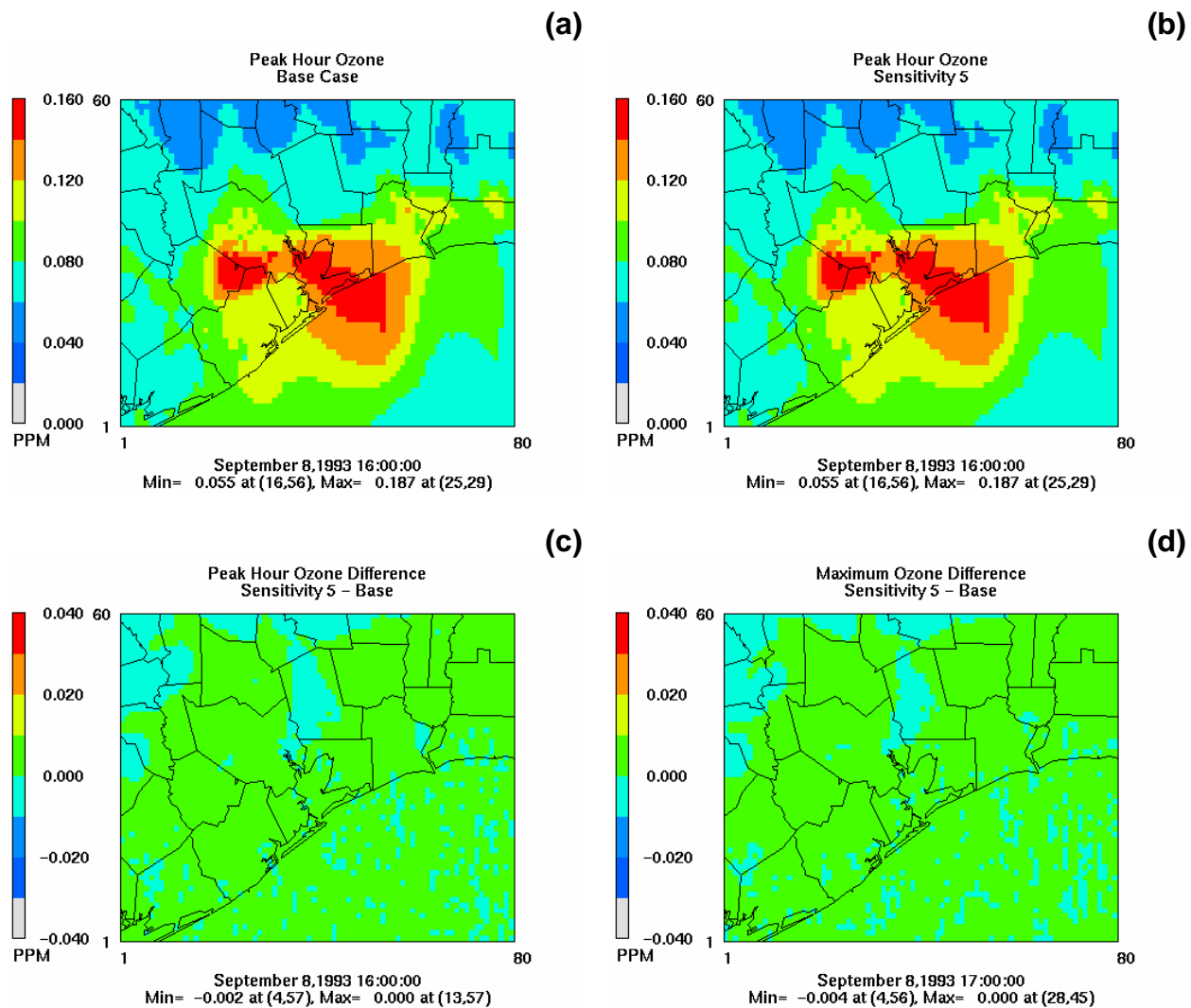


Figure 3-10. S5 results for September 8, 1993: (a) peak ozone concentration for base; (b) peak ozone concentration for sensitivity at base peak time; (c) ozone concentration difference (sensitivity-base) at peak hour for base; and (d) ozone concentration difference (sensitivity-base) at hour of maximum difference.

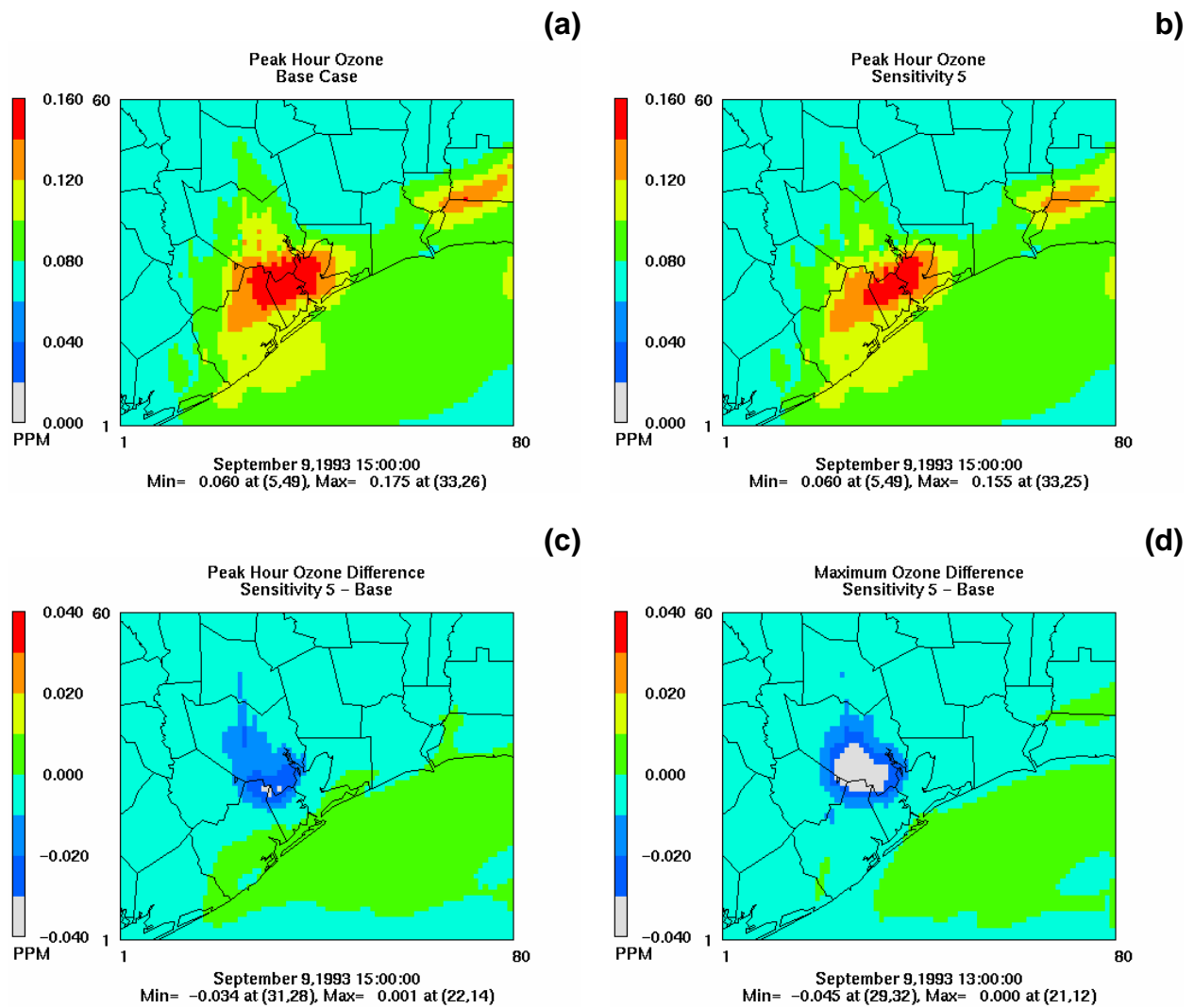


Figure 3-11. S5 results for September 9, 1993: (a) peak ozone concentration for base; (b) peak ozone concentration for sensitivity at base peak time; (c) ozone concentration difference (sensitivity-base) at peak hour for base; and (d) ozone concentration difference (sensitivity-base) at hour of maximum difference.

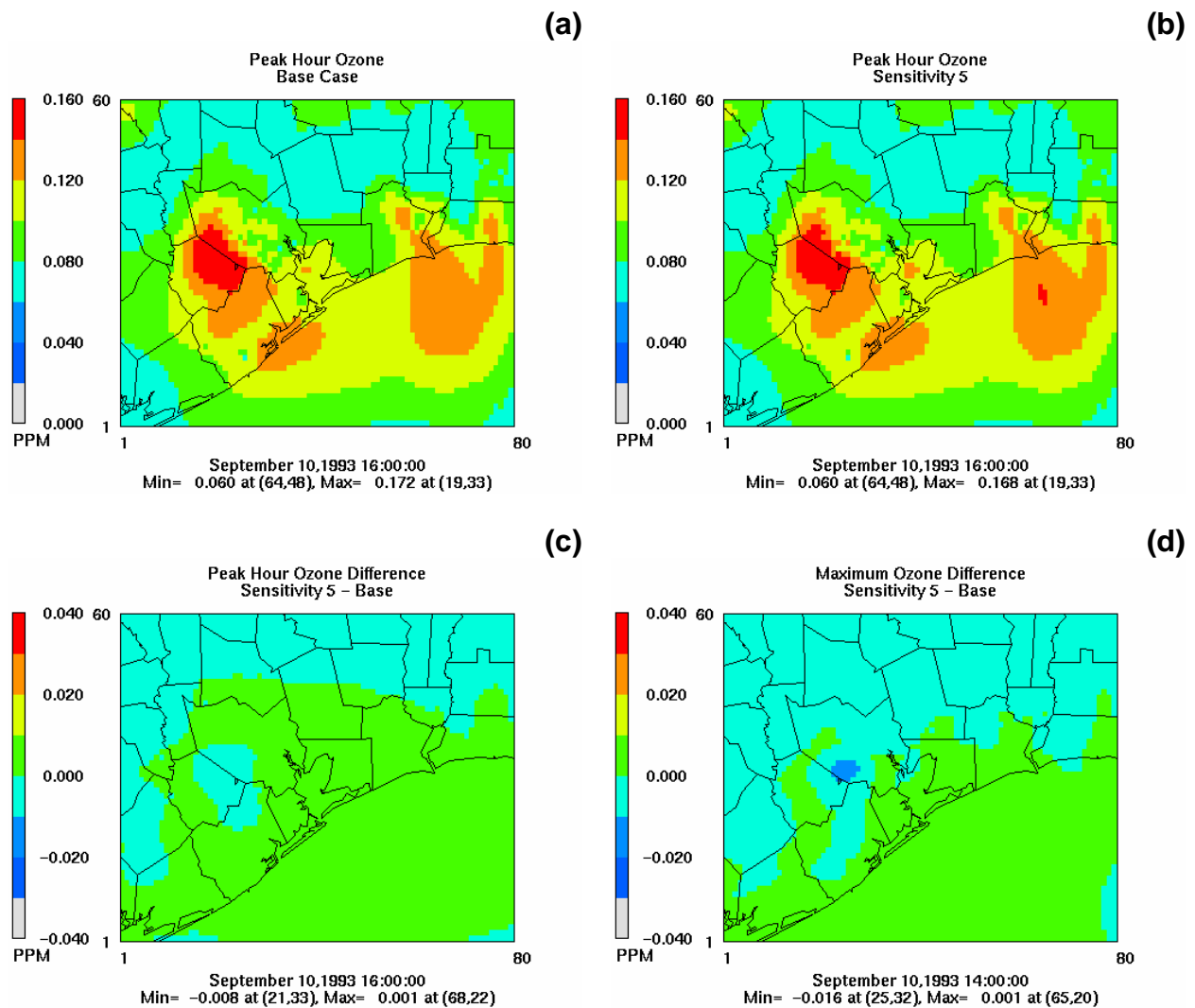


Figure 3-12. S5 results for September 10, 1993: (a) peak ozone concentration for base; (b) peak ozone concentration for sensitivity at base peak time; (c) ozone concentration difference (sensitivity-base) at peak hour for base; and (d) ozone concentration difference (sensitivity-base) at hour of maximum difference.

In S6 (**Figures 3-13 and 3-14**), removing the Houston core surface NO_x emissions has an effect in peak cell values as well as the extent of high concentrations of ozone. The difference between the peak cell for September 8 is 19 ppb, from 187 ppb to 168 ppb, and on September 10, 8 ppb, from 172 ppb to 164 ppb. The extent of the higher concentrations is more dramatically affected as the area of high concentrations shrinks, primarily along the urban core and some places east of the city. There are significant increases of ozone at nighttime over the urban core in comparison to the base case due to less titration by emitted NO_x . The concentration levels are generally low during the periods of reduced titration.

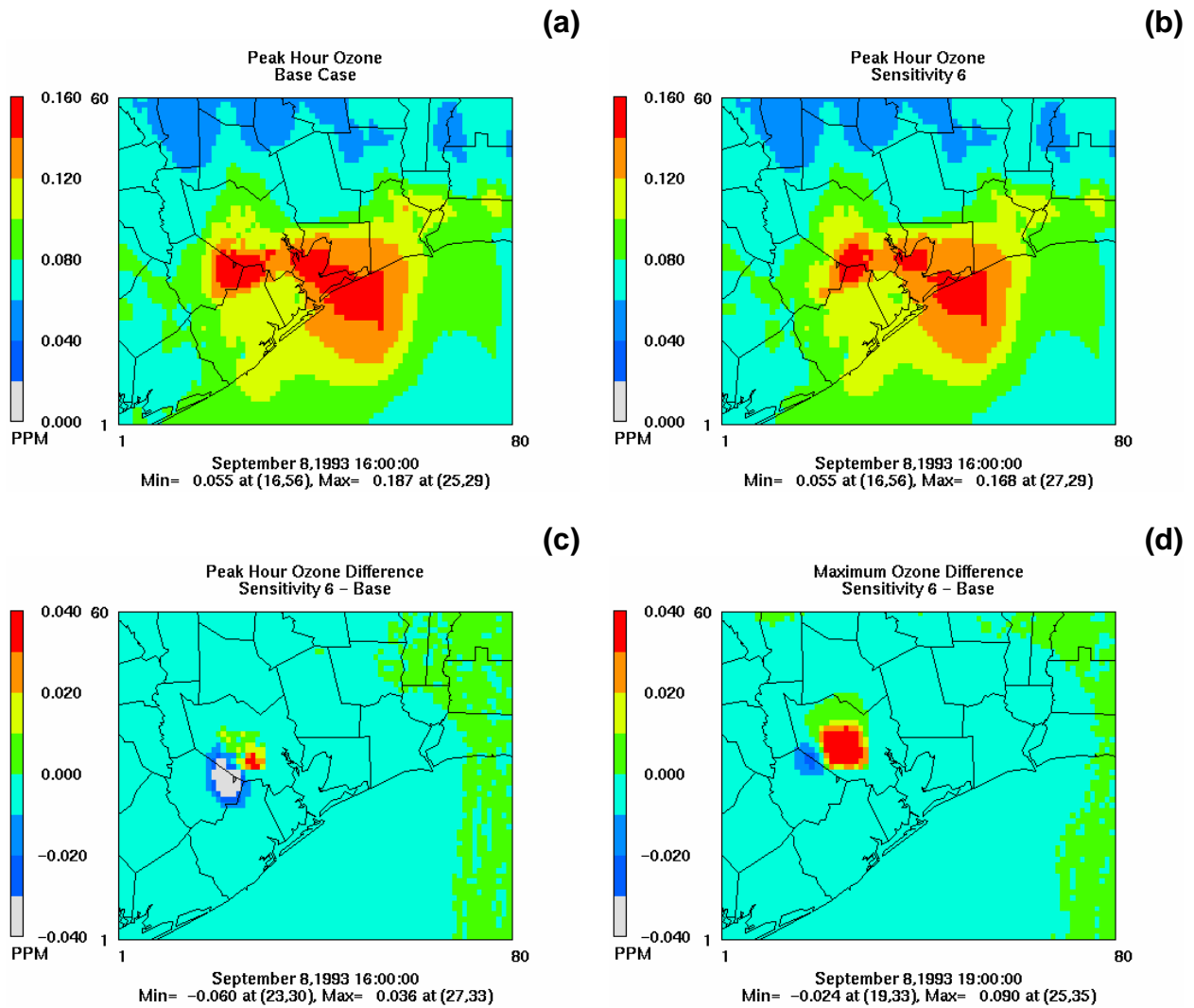


Figure 3-13. S6 results for September 8, 1993: (a) peak ozone concentration for base; (b) peak ozone concentration for sensitivity at base peak time; (c) ozone concentration difference (sensitivity-base) at peak hour for base; and (d) ozone concentration difference (sensitivity-base) at hour of maximum difference.

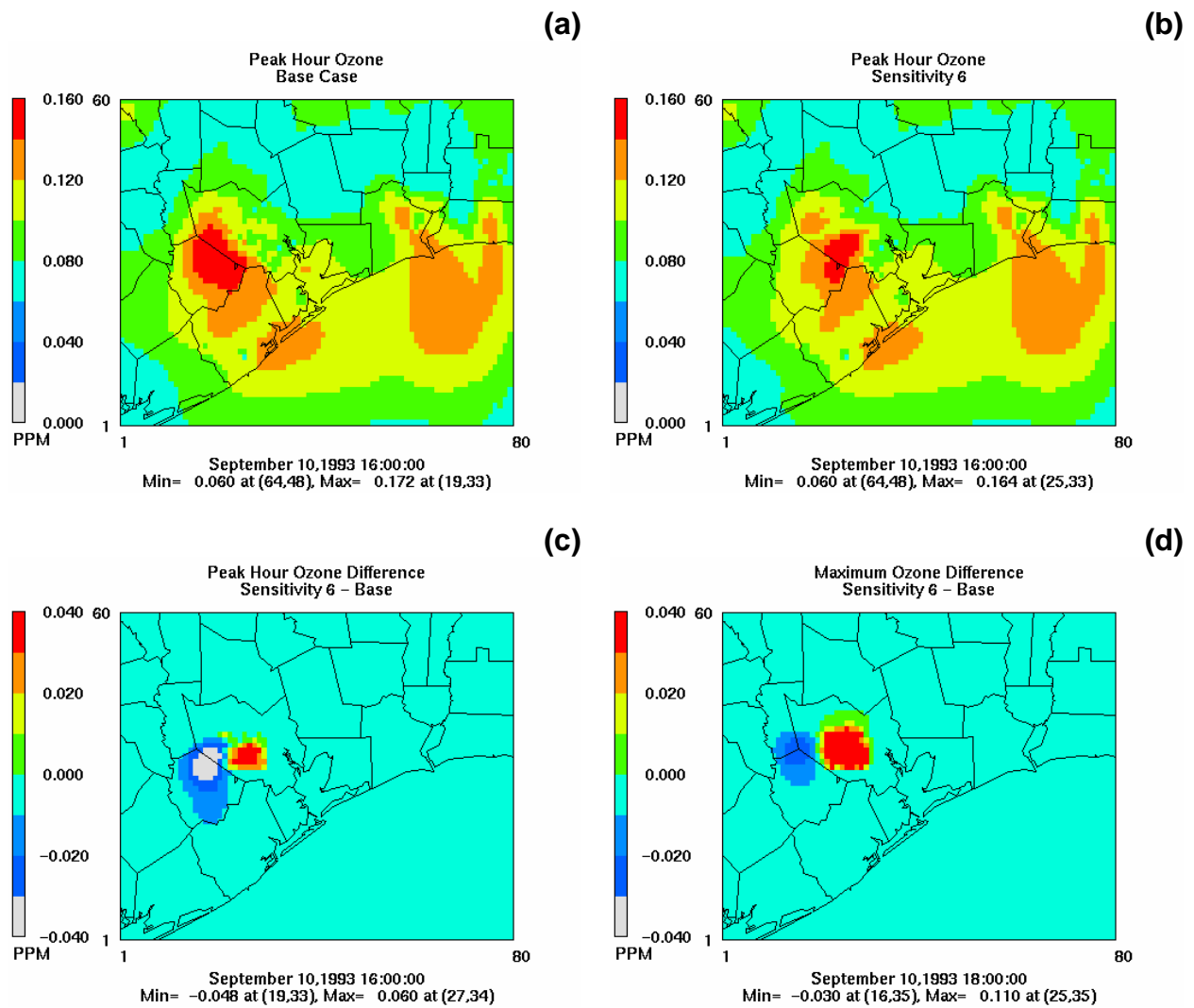


Figure 3-14. S6 results for September 10, 1993: (a) peak ozone concentration for base; (b) peak ozone concentration for sensitivity at base peak time; (c) ozone concentration difference (sensitivity-base) at peak hour for base; and (d) ozone concentration difference (sensitivity-base) at hour of maximum difference.

In S7 (**Figures 3-15 and 3-16**), the increased propylene and ethylene emissions at Chocolate Bayou and Texas City have little effect on the peak concentrations in the city. The increase in the peak cell for September 8 is 1 ppb, from 187 ppb to 188 ppb, and on September 10, there is no change in the peak cell value. However, there is an increase in areas exceeding 140 ppb. The largest ozone increases are in the regions local to Chocolate Bayou and Texas City. In addition, transport into the Gulf is evident where the largest increases in ozone concentration are seen.

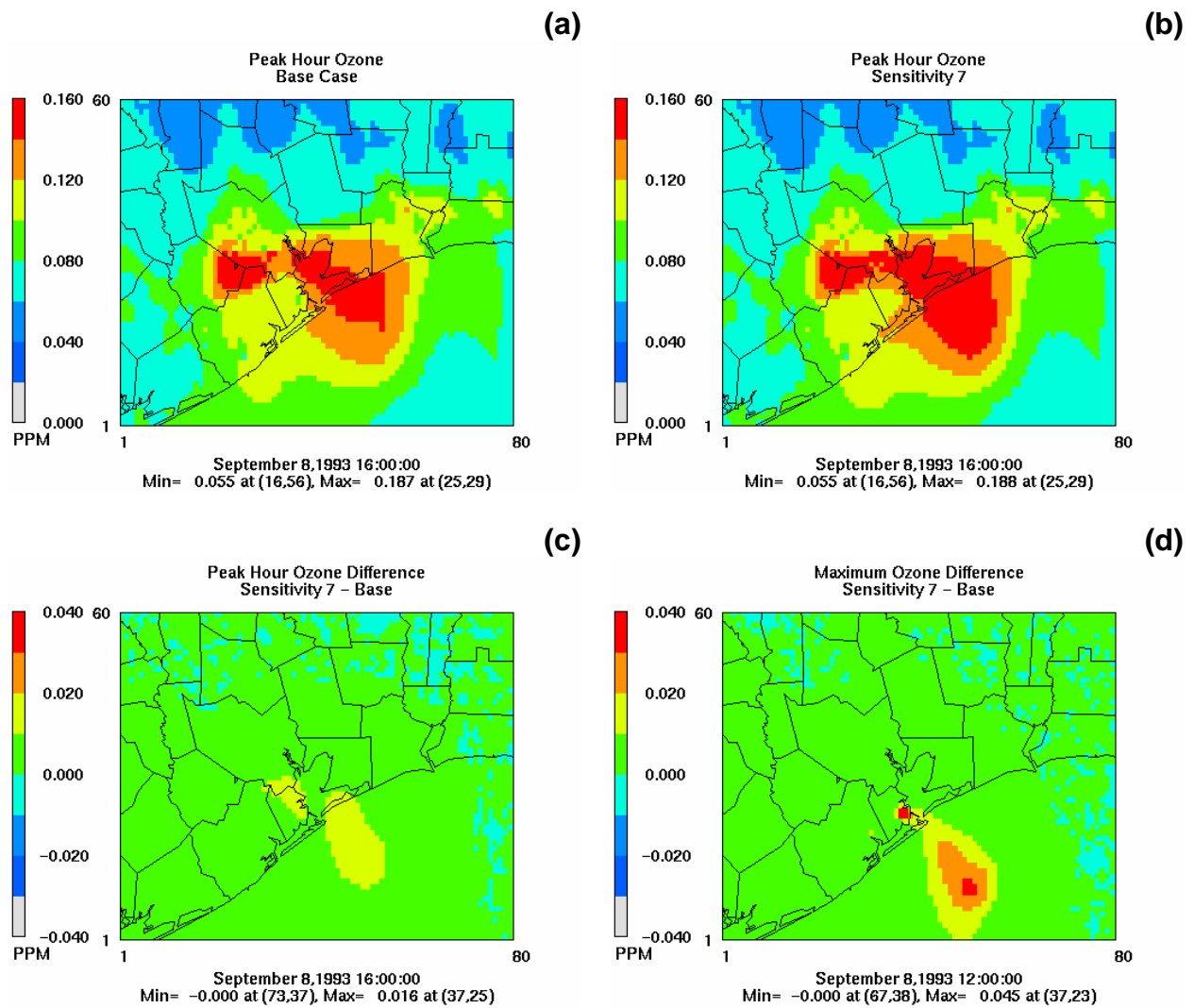


Figure 3-15. S7 results for September 8, 1993: (a) peak ozone concentration for base; (b) peak ozone concentration for sensitivity at base peak time; (c) ozone concentration difference (sensitivity-base) at peak hour for base; and (d) ozone concentration difference (sensitivity-base) at hour of maximum difference.

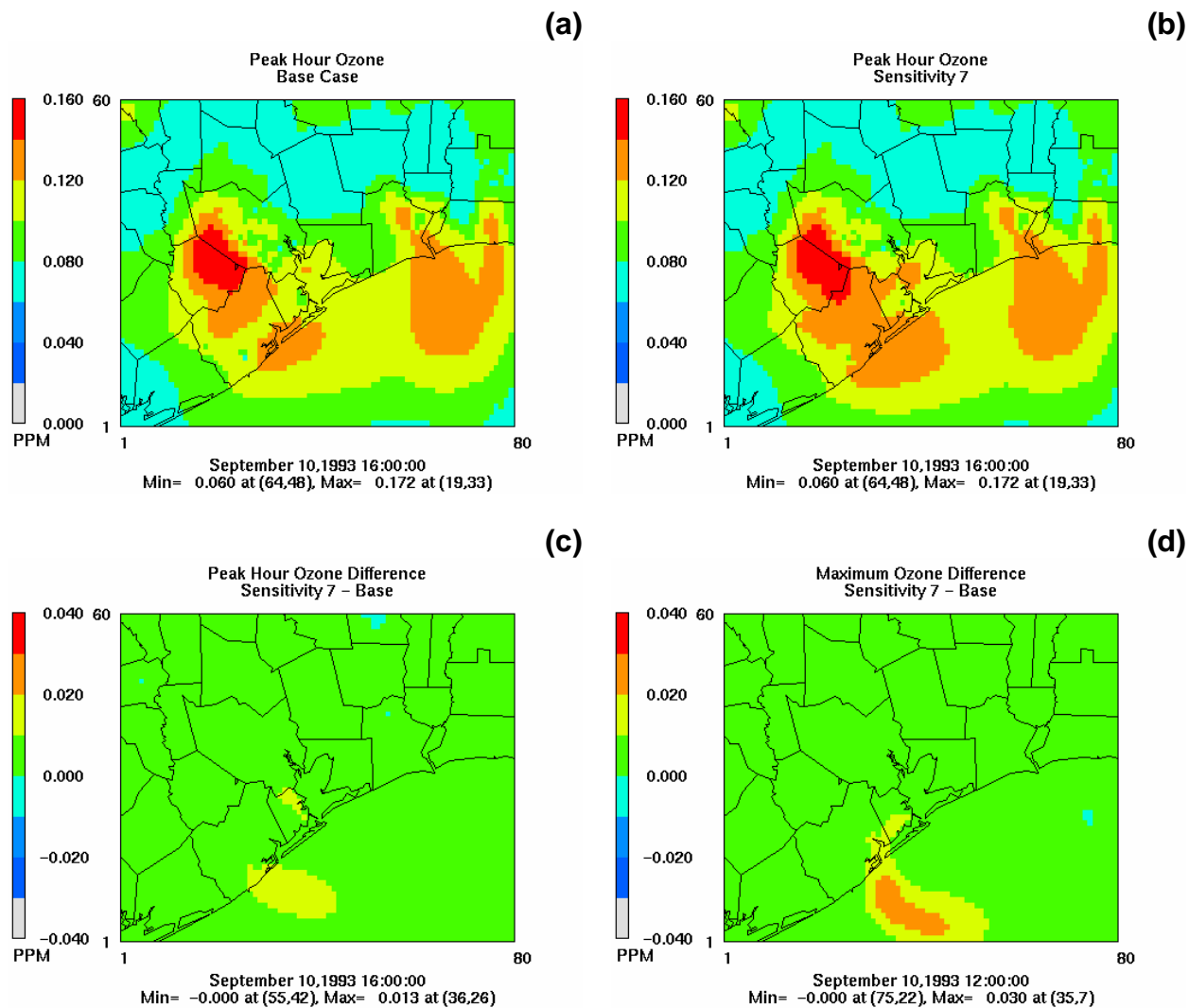


Figure 3-16. S7 results for September 10, 1993: (a) peak ozone concentration for base; (b) peak ozone concentration for sensitivity at base peak time; (c) ozone concentration difference (sensitivity-base) at peak hour for base; and (d) ozone concentration difference (sensitivity-base) at hour of maximum difference.

In S8, (**Figure 3-17, 3-18, and 3-19**), clouds are introduced with a 50% NO_x emission reduction domain-wide; and the results are similar to S5 when comparing to the base case. When comparing to S5 as in Figures 3-17, 3-18, and 3-19, the effects discussed for S5 are appropriate—the clouds diminish the peak concentrations slightly, and there are some more significant effects on other cells during the simulation, up to a 37 ppb decrease in ozone concentrations due to reduced photolysis.

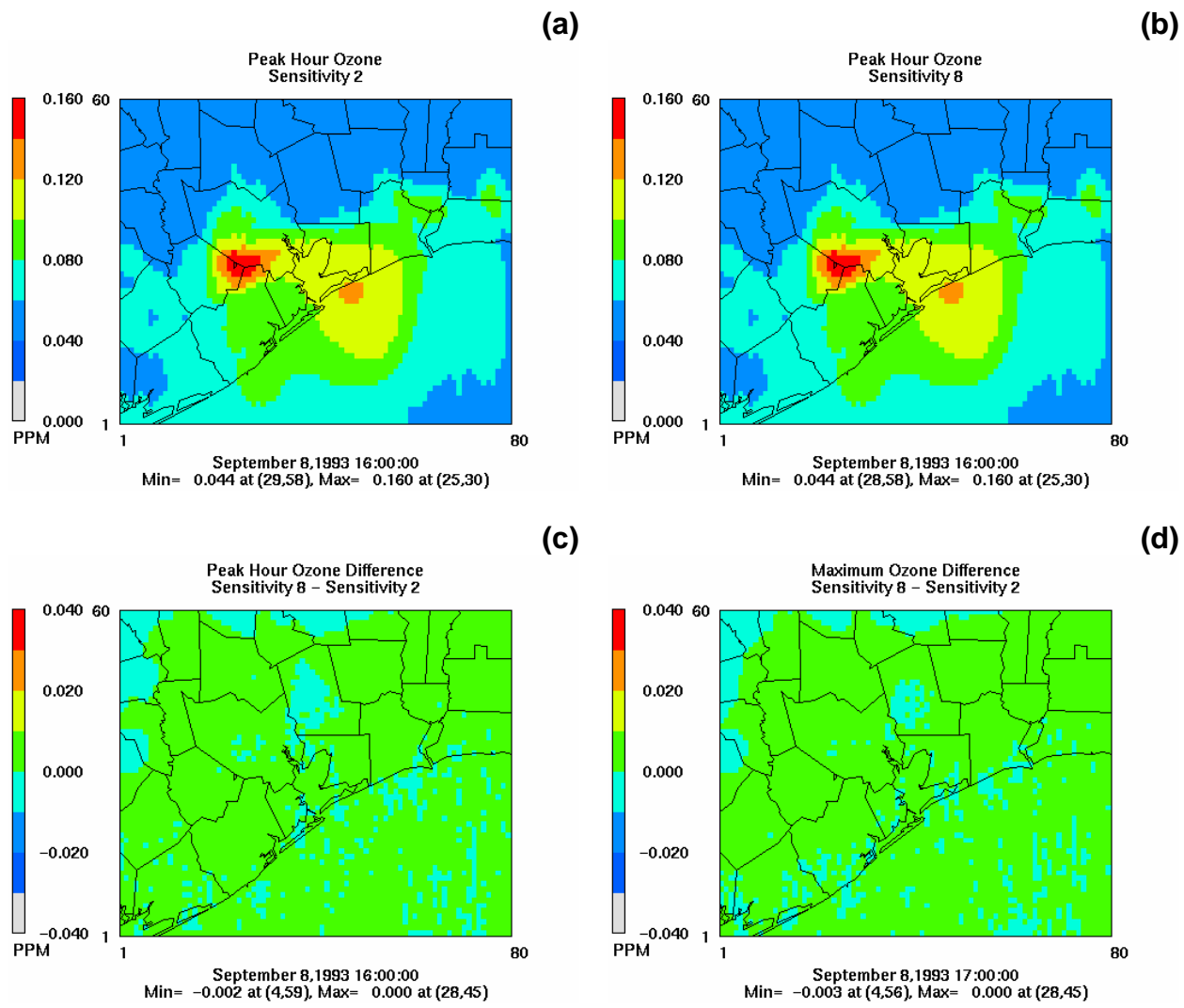


Figure 3-17. S8 results for September 8, 1993: (a) peak ozone concentration for S5; (b) peak ozone concentration for Sensitivity 8 at the S5 peak time; (c) ozone concentration difference (S8-S5) at the S5 peak hour; and (d) ozone concentration difference (S8-S5) at hour of maximum difference.

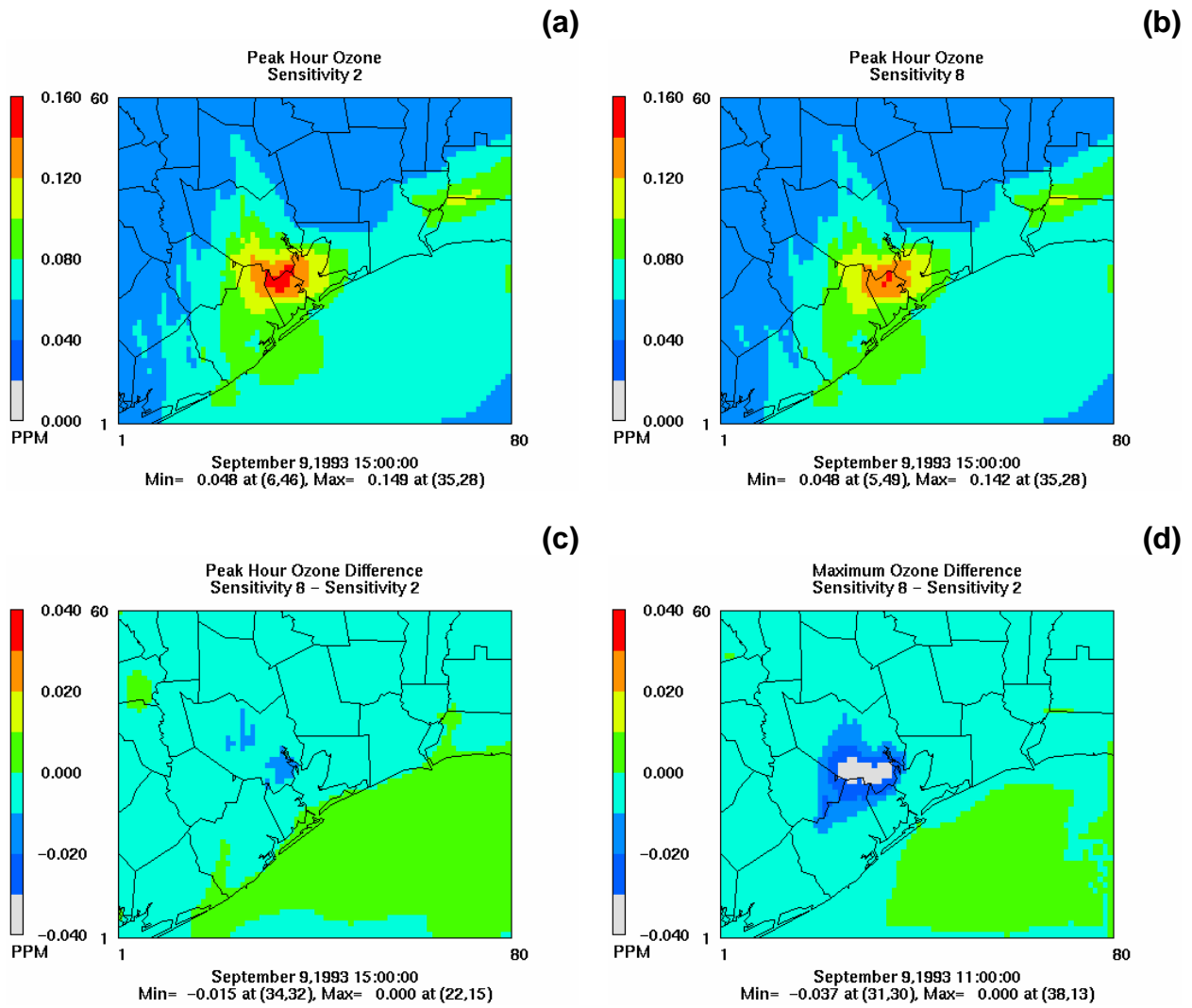


Figure 3-18. S8 results for September 9, 1993: (a) peak ozone concentration for S5; (b) peak ozone concentration for S8 at the S5 peak time; (c) ozone concentration difference (S8-S5) at the S5 peak hour; and (d) ozone concentration difference (S8-S5) at hour of maximum difference.

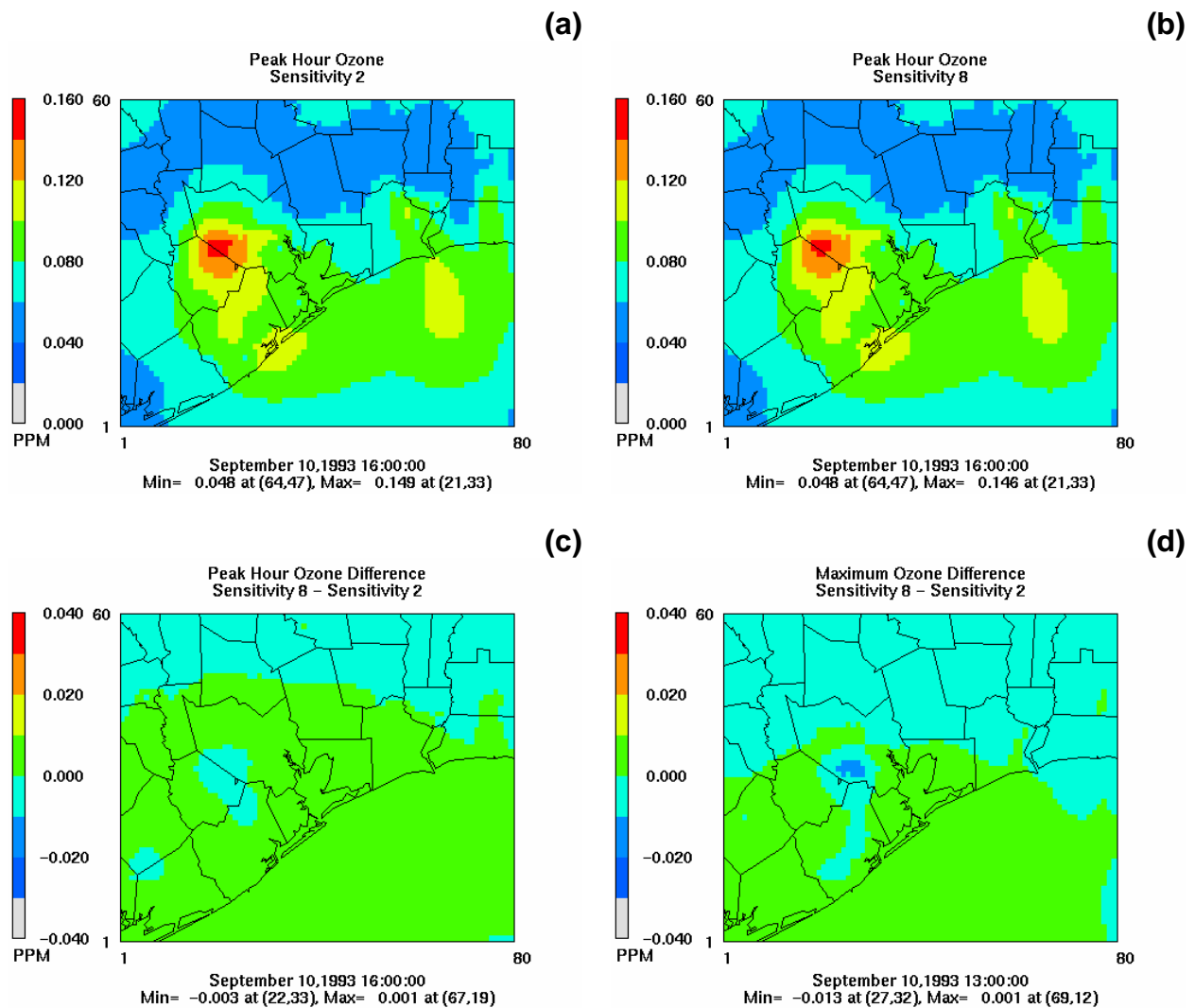


Figure 3-19. S8 results for September 10, 1993: (a) peak ozone concentration for S5; (b) peak ozone concentration for S8 at the S5 peak time; (c) ozone concentration difference (S8-S5) at the S5 peak hour; and (d) ozone concentration difference (S8-S5) at hour of maximum difference.

In S9 (Figures 3-20 and 3-21), the increased propylene and ethylene emissions in the Ship Channel have an effect on peak concentrations. The increase in the peak cell for September 8 is 12 ppb, from 187 ppb to 199 ppb, and on September 10, 5 ppb, from 172 ppb to 177 ppb. Likewise, there is an expansion of the regions exceeding 140 ppb. The greatest increases during the day are away from shore, likely due to the transport direction at that time. Again, there are increases in ozone concentrations domain-wide.

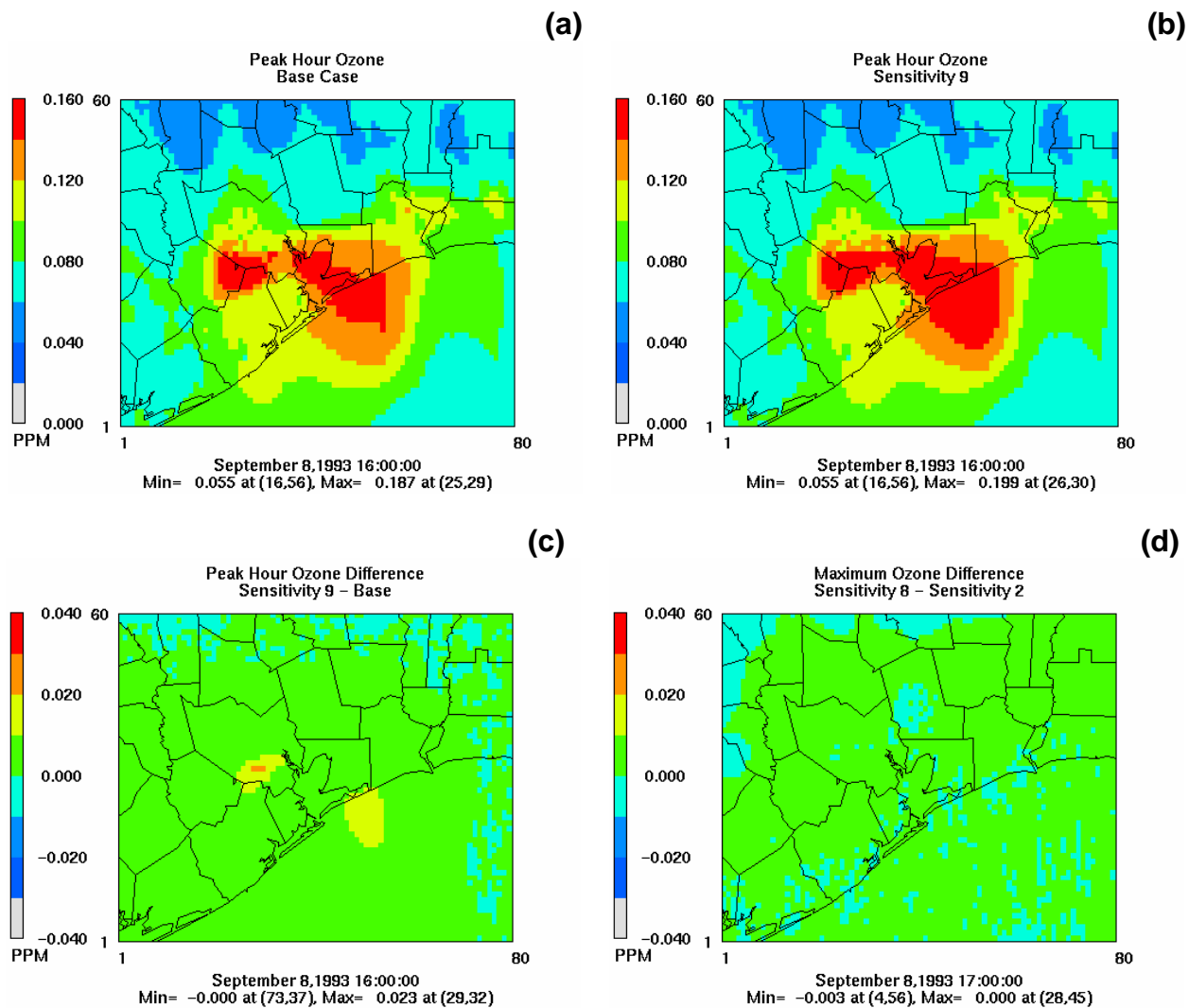


Figure 3-20. S9 results for September 8, 1993: (a) peak ozone concentration for base; (b) peak ozone concentration for sensitivity at base peak time; (c) ozone concentration difference (sensitivity-base) at peak hour for base; and (d) ozone concentration difference (sensitivity-base) at hour of maximum difference.

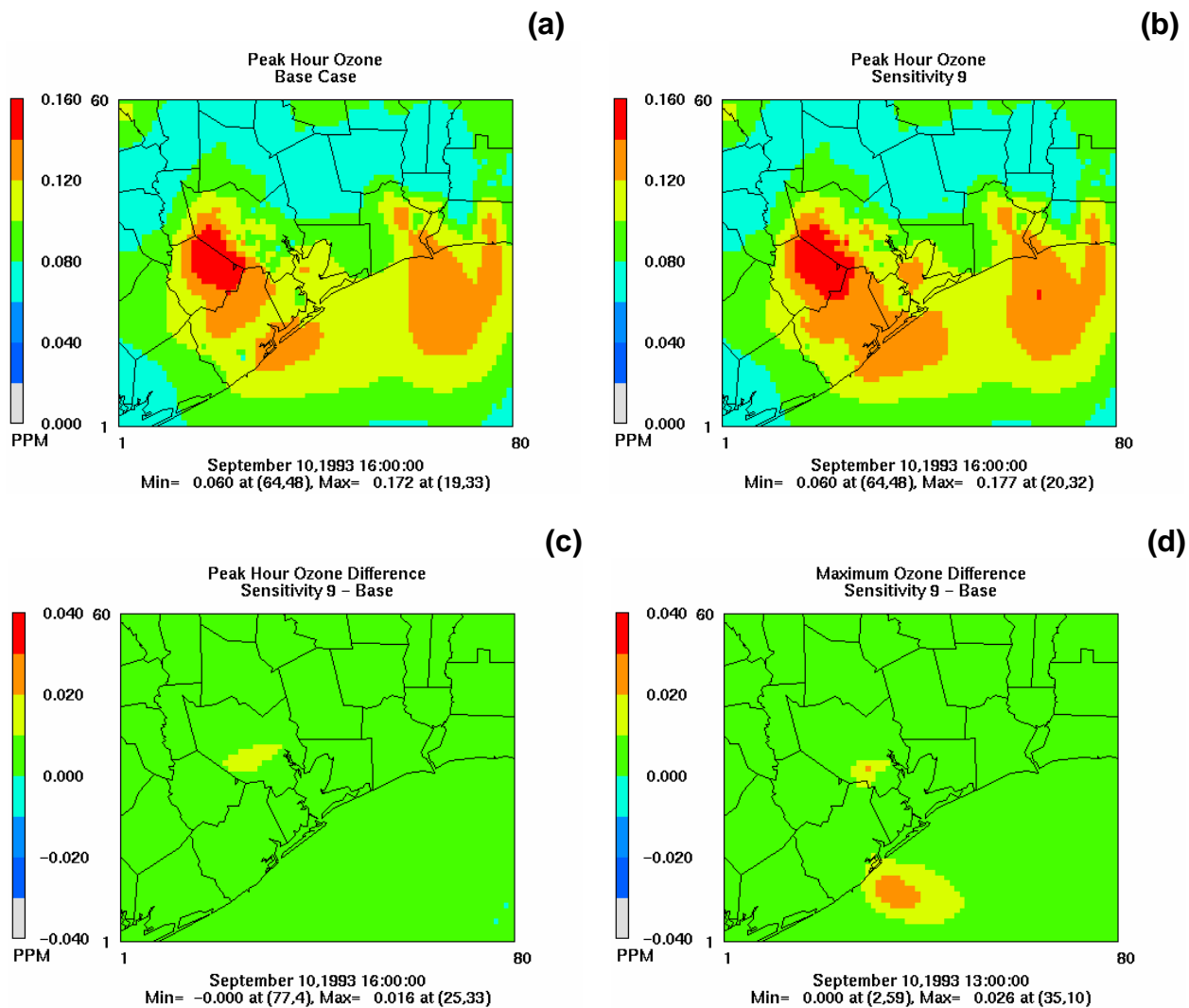


Figure 3-21. S9 results for September 10, 1993: (a) peak ozone concentration for base; (b) peak ozone concentration for sensitivity at base peak time; (c) ozone concentration difference (sensitivity-base) at peak hour for base; and (d) ozone concentration difference (sensitivity-base) at hour of maximum difference.

In S10 (Figures 3-22 and 3-23), decreases in the wind speed with increased propylene and ethylene emissions at Chocolate Bayou and Texas City have a significant effect on the peak concentrations in the Houston area. The increase in the peak cell for September 8 is 17 ppb, from 187 ppb to 204 ppb, and on September 10, 12 ppb, from 172 ppb to 184 ppb. Likewise, the expansion of the regions with concentration above 140 ppb is significant when compared to the base case. In comparison to S7, the reduced wind speed produces increases in the peak cells on September 8 of 16 ppb, from 188 ppb to 204 ppb, and on September 10, increases of 12 ppb, from 172 ppb to 184 ppb. However, the effect of reduced wind speeds on the Texas City plume is small, and the effect on the Chocolate Bayou plume is most pronounced when the winds are offshore. The effect on Chocolate Bayou can be seen offshore in Figure 3-21(d).

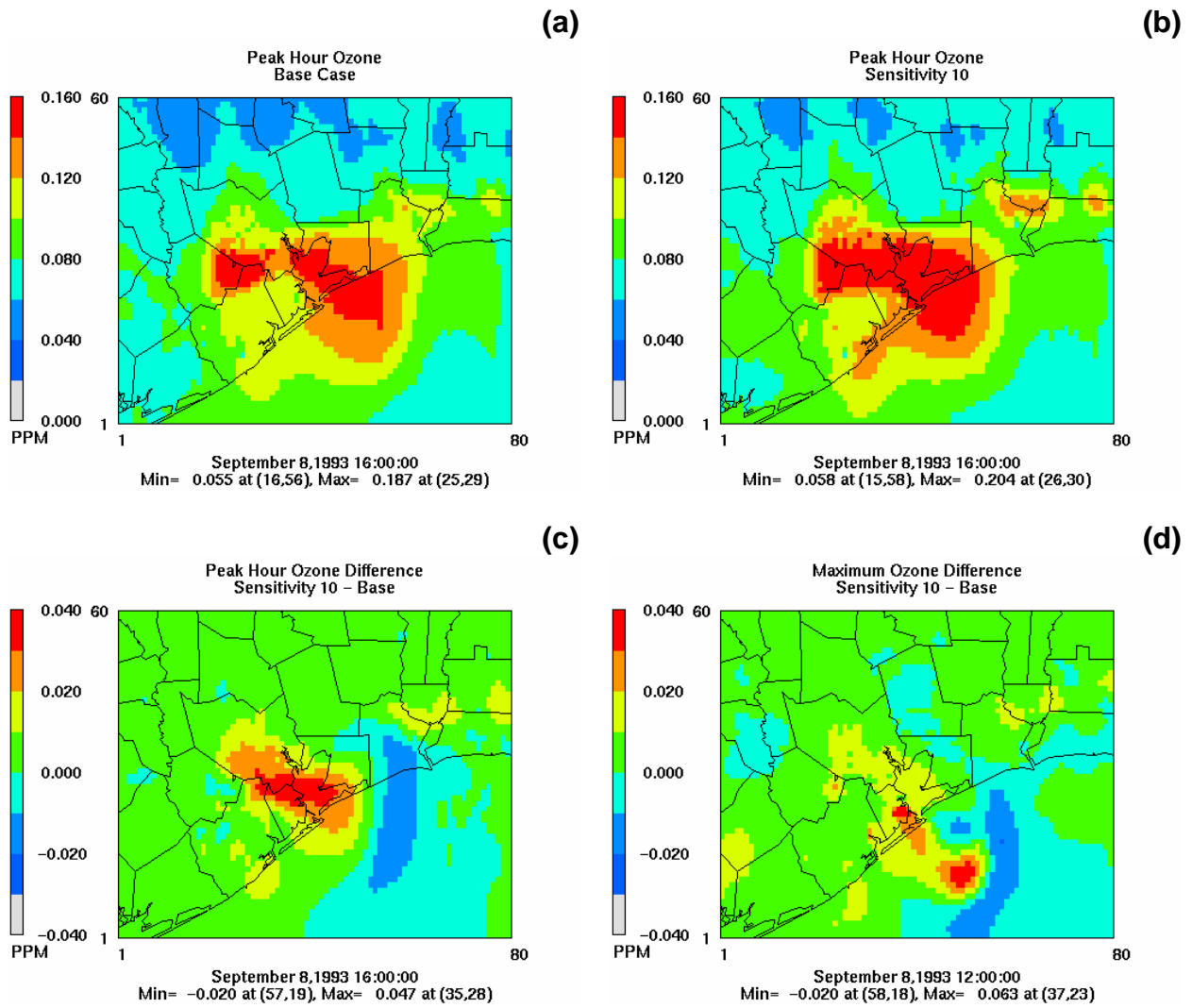


Figure 3-22. S10 results for September 8, 1993: (a) peak ozone concentration for base; (b) peak ozone concentration for sensitivity at base peak time; (c) ozone concentration difference (sensitivity-base) at peak hour for base; and (d) ozone concentration difference (sensitivity-base) at hour of maximum difference.

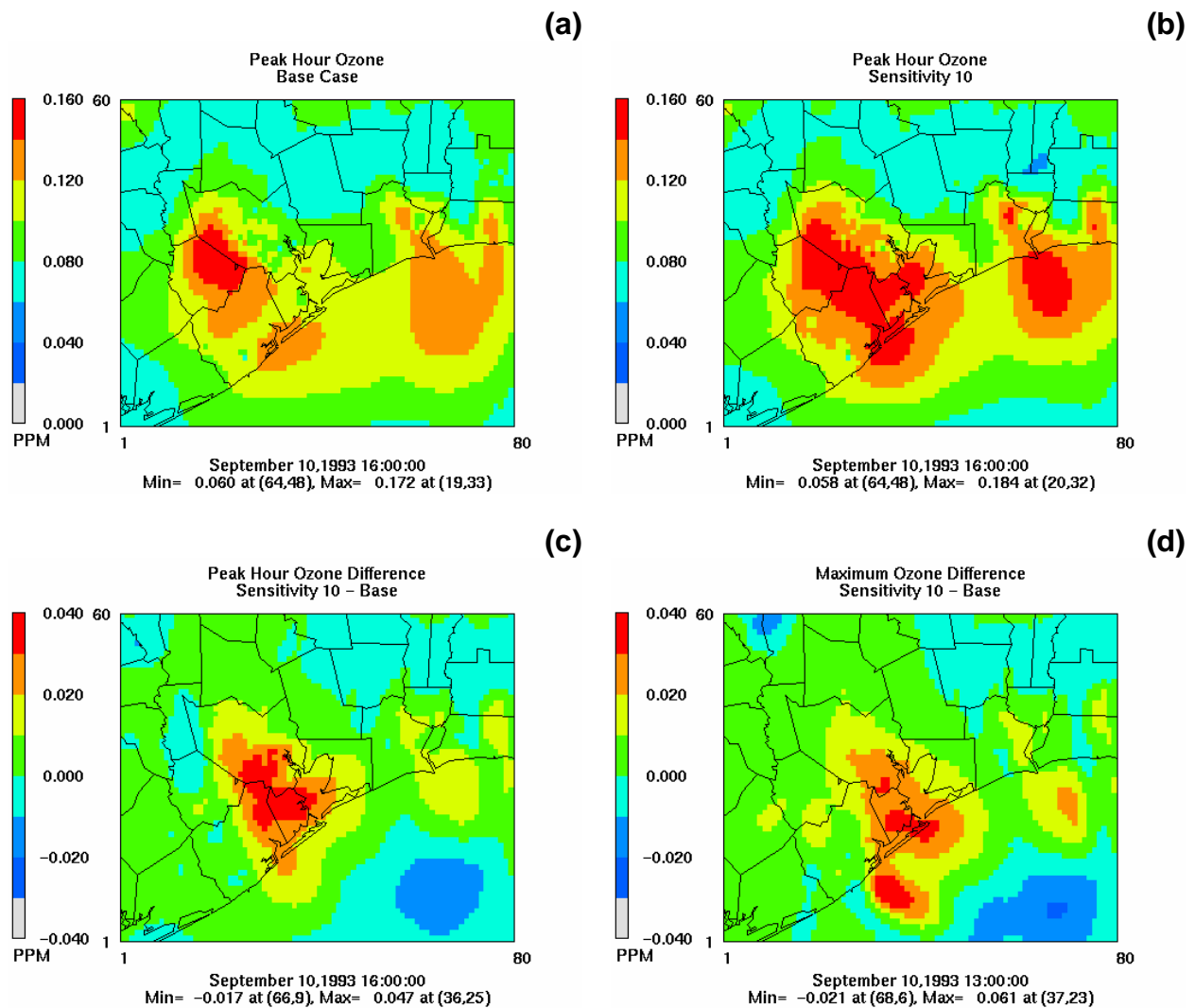


Figure 3-23. S10 results for September 10, 1993: (a) peak ozone concentration for base; (b) peak ozone concentration for sensitivity at base peak time; (c) ozone concentration difference (sensitivity-base) at peak hour for base; and (d) ozone concentration difference (sensitivity-base) at hour of maximum difference.

In S11 (**Figures 3-24 and 3-25**), the decreased vertical diffusion coefficient K_v with the increased propylene and ethylene emissions at Chocolate Bayou and Texas City has a very small effect on the peak concentrations when compared to the base case. The increase in the peak cell for September 8 is 2 ppb, from 187 ppb to 189 ppb, and on September 10, 2 ppb, from 172 ppb to 174 ppb. In comparison to S7, the reduced K_v causes increases in the peak cells on September 8 of 1 ppb, from 188 ppb to 189 ppb, and on September 10, increases of 2 ppb, from 172 ppb to 174 ppb. The model is not very sensitive to a 25% decrease in this coefficient.

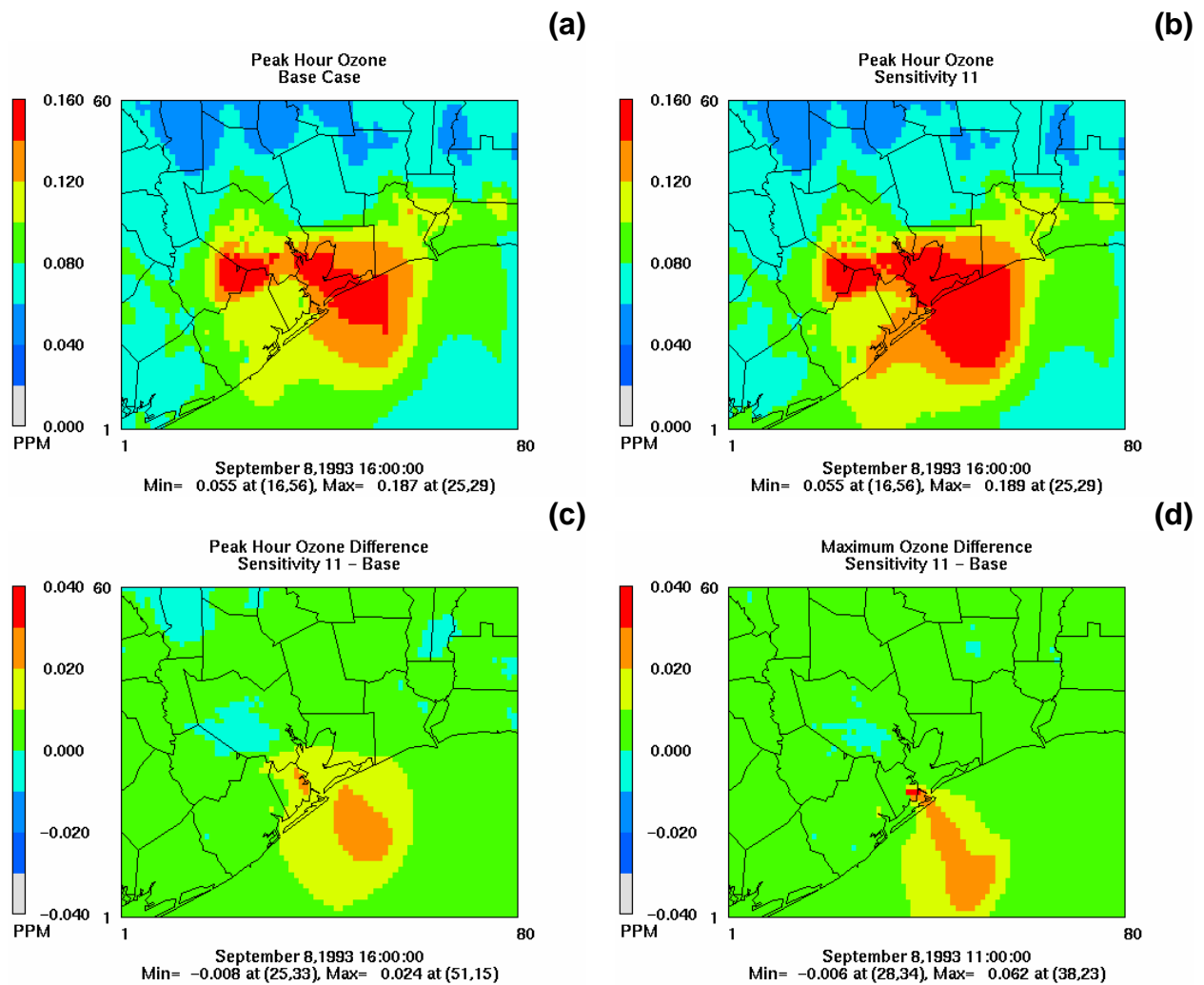


Figure 3-24. S11 results for September 8, 1993: (a) peak ozone concentration for base; (b) peak ozone concentration for sensitivity at base peak time; (c) ozone concentration difference (sensitivity-base) at peak hour for base; and (d) ozone concentration difference (sensitivity-base) at hour of maximum difference.

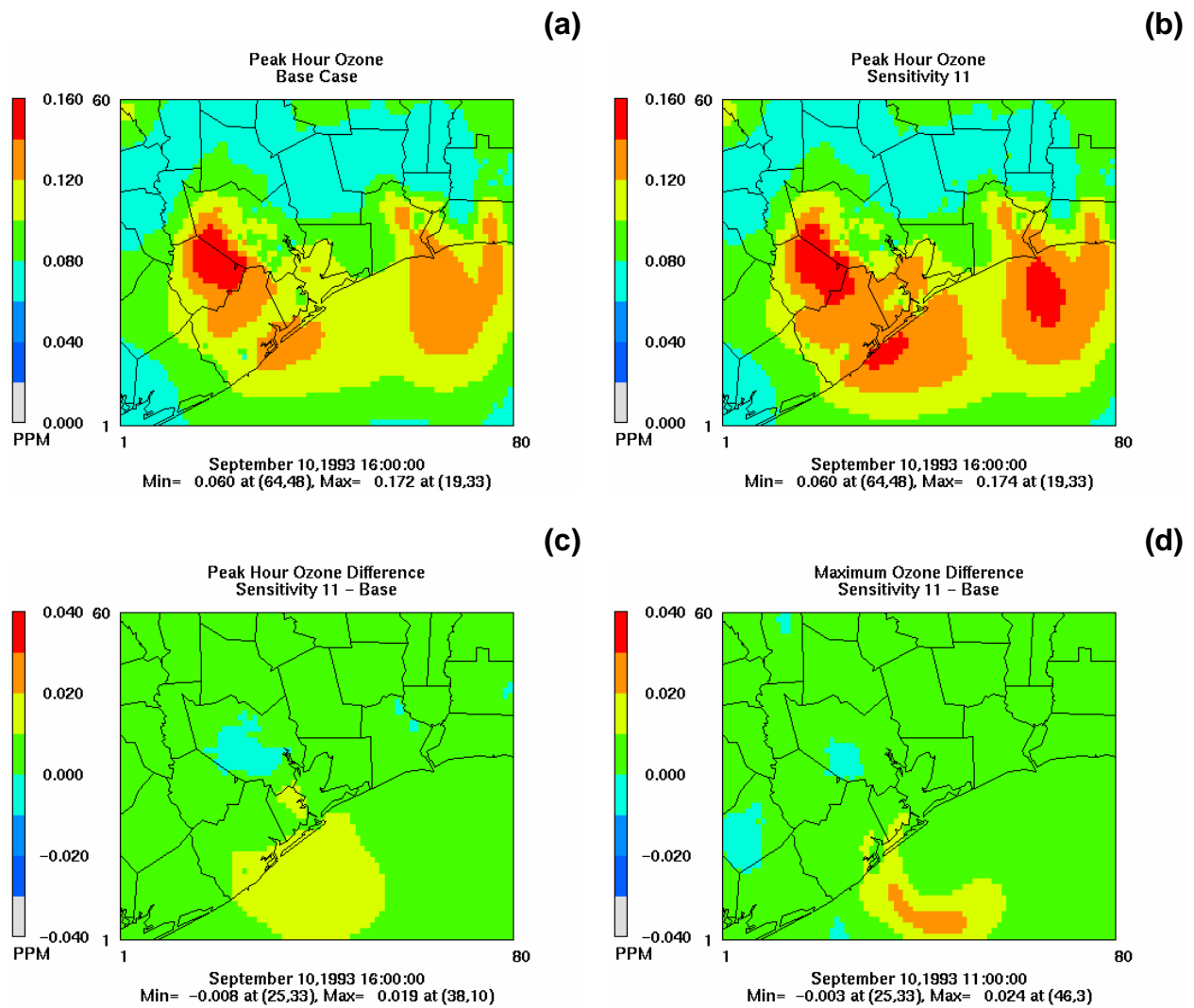


Figure 3-25. S11 results for September 10, 1993: (a) peak ozone concentration for base; (b) peak ozone concentration for sensitivity at base peak time; (c) ozone concentration difference (sensitivity-base) at peak hour for base; and (d) ozone concentration difference (sensitivity-base) at hour of maximum difference.

In S12, the spike chemical event of OLE and ETH created as much as a 10 ppb increase in the ozone concentrations. However, these increases were localized to the vicinity of Chocolate Bayou and dissipated as they were transported away in later hours. The increases had little effect on the peak concentration in the Houston area. These results are discussed further in Section 3.3, Spike Intensity.

3.2 CLOUD COVER EFFECTS

Clear sky has been assumed for prior CAMx simulations of the HGA September 1993 ozone episode. A sensitivity simulation with clouds was run. CAMx cloud cover input files were prepared for September 8, 9, and 10, 1993. The procedures used to prepare the cloud cover input files are described in Section 2. The input files are UAM-V type CLOUD file. Within CAMx, clear sky photolysis rates are adjusted as a function of cloud fraction specified in those files. Cloud effects on temperature or other meteorological parameters were not considered. Cloud cover varied over the time period: September 8 had the least cloud cover and September 9, the most cloud cover.

September 8 had clear sky onshore within the fine grid domain until 1030 CST. Overcast clouds moved into the northwest corner of the grid domain midmorning and remained the rest of the day. Scattered clouds formed overland by 1430 CST, remaining mostly to the northwest of Houston. Some scattered clouds occurred over Harris County after 1400 CST. The sky remained clear all day over Trinity Bay and offshore in the Gulf of Mexico. **Figure 3-26** shows the cloud fraction at 1200 CST on September 8, 1993.

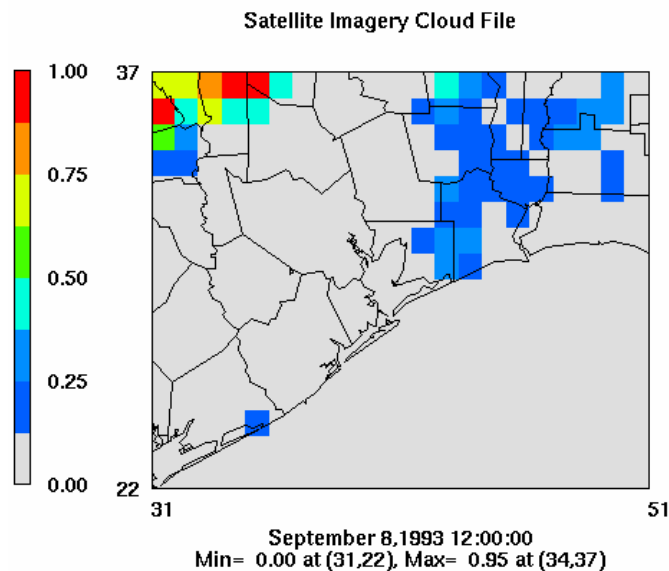


Figure 3-26. Cloud fraction on September 8, 1993.

On the morning of September 9, overcast sky covered the Houston area extending southwest to northeast parallel to the coastline. The sky began clearing over Houston about 1200 CST with the overcast moving to the northeast. Scattered clouds remained over Houston until late afternoon. Immediately offshore in the Gulf of Mexico the sky was clear all day. **Figure 3-27** shows the cloud fraction at 1200 CST on September 9, 1993.

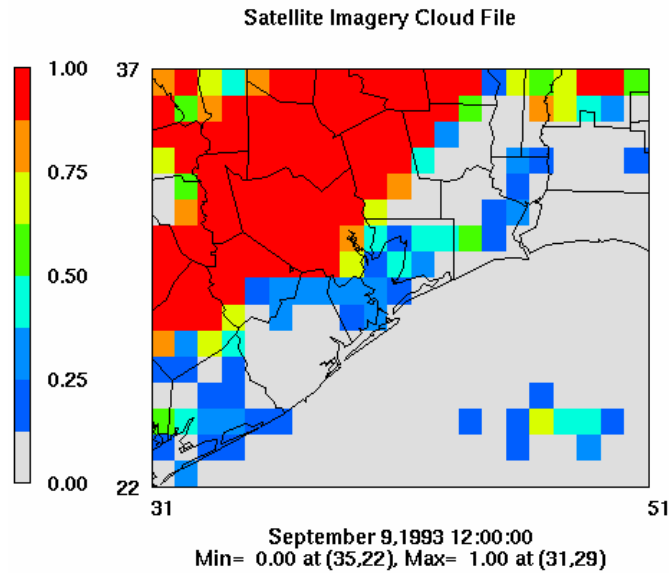


Figure 3-27. Cloud fraction on September 9, 1993 at 1200 CST.

On the morning of September 10, a small area of overcast sky was northwest of Harris County. The sky was also overcast far offshore in the Gulf of Mexico. The Houston area remained clear until 1200 CST. Scattered clouds then formed over land while the sky remained clear offshore and over Trinity and Galveston Bays. The sky cleared somewhat over Houston after 1400 CST. **Figure 3-28** shows the cloud fraction at 1200 CST on September 10, 1993.

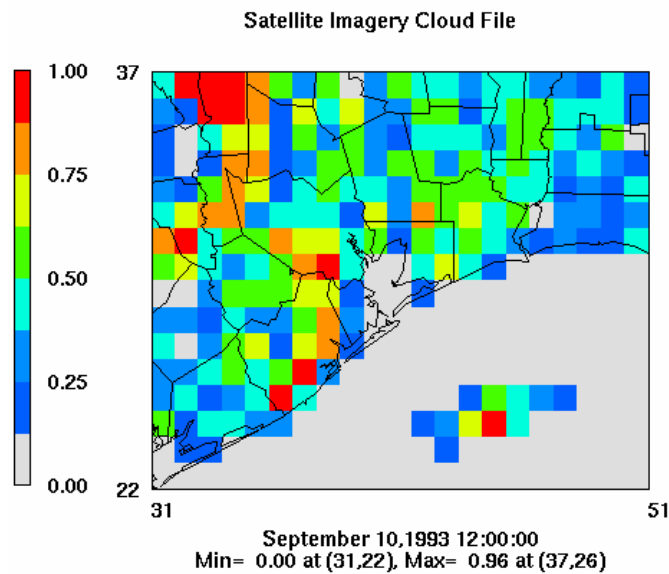


Figure 3-28. Cloud fraction on September 10, 1993 at 1200 CST.

Cloud cover did not have a significant effect on ozone generation on September 8. The base-case daily peak predicted ozone was 0.187 ppm at 1600 CST. This predicted peak ozone remained unchanged in the cloud cover sensitivity simulation. There was a small decrease of 4 ppb in ozone at 1700 CST in the northwest corner of the fine grid, the area with overcast sky. Elsewhere within the fine grid domain, ozone decreased less than 1 ppb. Model performance on this day should not have been affected by the input of clouds.

The cloud cover on September 9 inhibited ozone production in the morning in Harris County and to the southwest. At 1000 CST, predicted ozone in the cloud sensitivity simulation was 20 ppb less than the base case in the Houston area. The maximum effect of the cloud cover in the Houston area occurred at 1300 CST when predicted ozone was 45 ppb less than in the base case. **Figure 3-29** shows the difference (sensitivity – base) between the base-case modeled ozone and the cloud sensitivity simulation at 1300 CST. At 1600 CST, the time of peak predicted ozone, the effect of clouds was smaller with only a maximum 27 ppb decrease in ozone. **Figure 3-30** shows the difference at 1600 CST. The area of ozone deficit moved north during the night to southern Montgomery County with the difference from the base slowly decreasing to 8 ppb by 2300 CST.

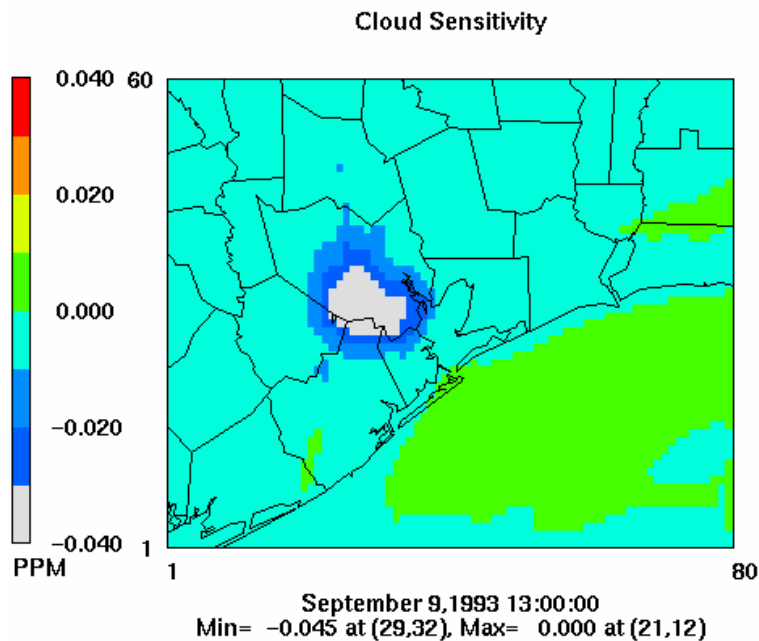


Figure 3-29. Cloud sensitivity ozone difference (sensitivity – base) at 1300 CST on September 9, 1993.

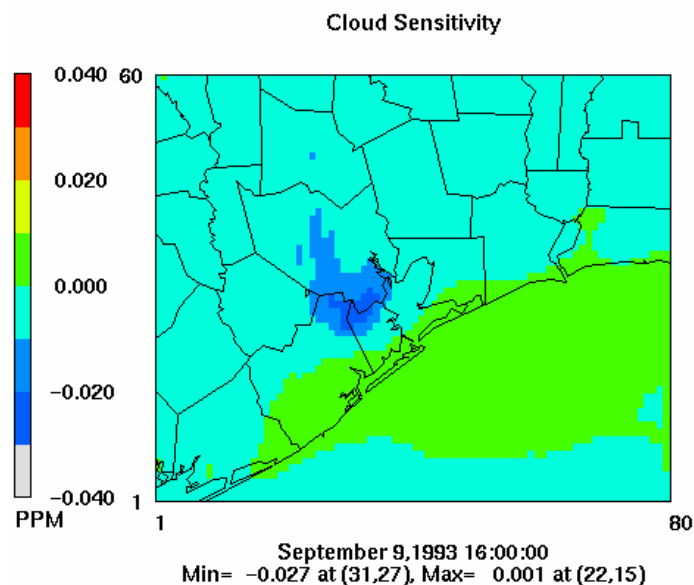


Figure 3-30. Cloud sensitivity ozone difference (sensitivity – base) at 1600 CST on September 9, 1993.

The base-case simulation overpredicted observed ozone in central and western Houston on September 9. Along the Gulf Coast, ozone was underpredicted. For example, at the monitoring site at Croquet (HCQA) the base-case predicted peak ozone was 133 ppb in the HCQA grid cell while the observed peak ozone was about 93 ppb. This overprediction in western and central Houston was reduced in the cloud sensitivity simulation. Predicted peak ozone in the HCQA grid cell was 107 ppb in the cloud sensitivity simulation. The time series of ozone for the base case and the cloud sensitivity simulations at the grid cell where the HCQA monitor is located are shown in **Figure 3-31b**. Modeled ozone was unaffected by cloud cover at Smith Point (SPTC) to the east of Houston where ozone was underpredicted. The ozone time series for SPTC is shown in **Figure 3-31h**. Other underpredicted sites such as Texas City and Gilchrist (GLRC) were also unchanged. The base case predicted peak observed ozone at Seabrook (SBRC) very well. However, the cloud cover sensitivity simulation predicted 22 ppb less ozone than the base case causing an underprediction. The SBRC ozone time series is shown in **Figure 3-31g**.

The cloud cover has the greatest effect on modeled ozone in the morning hours, which is seen in the ozone time series plots in **Figure 3-31**. Model performance for predicting peak ozone should be improved in the cloud sensitivity simulation for those monitoring sites in central and western Houston that were overpredicted. However, there was some remaining overprediction and continued underprediction near the Gulf Coast; the timing of the inland transport by the sea breeze is a likely factor.

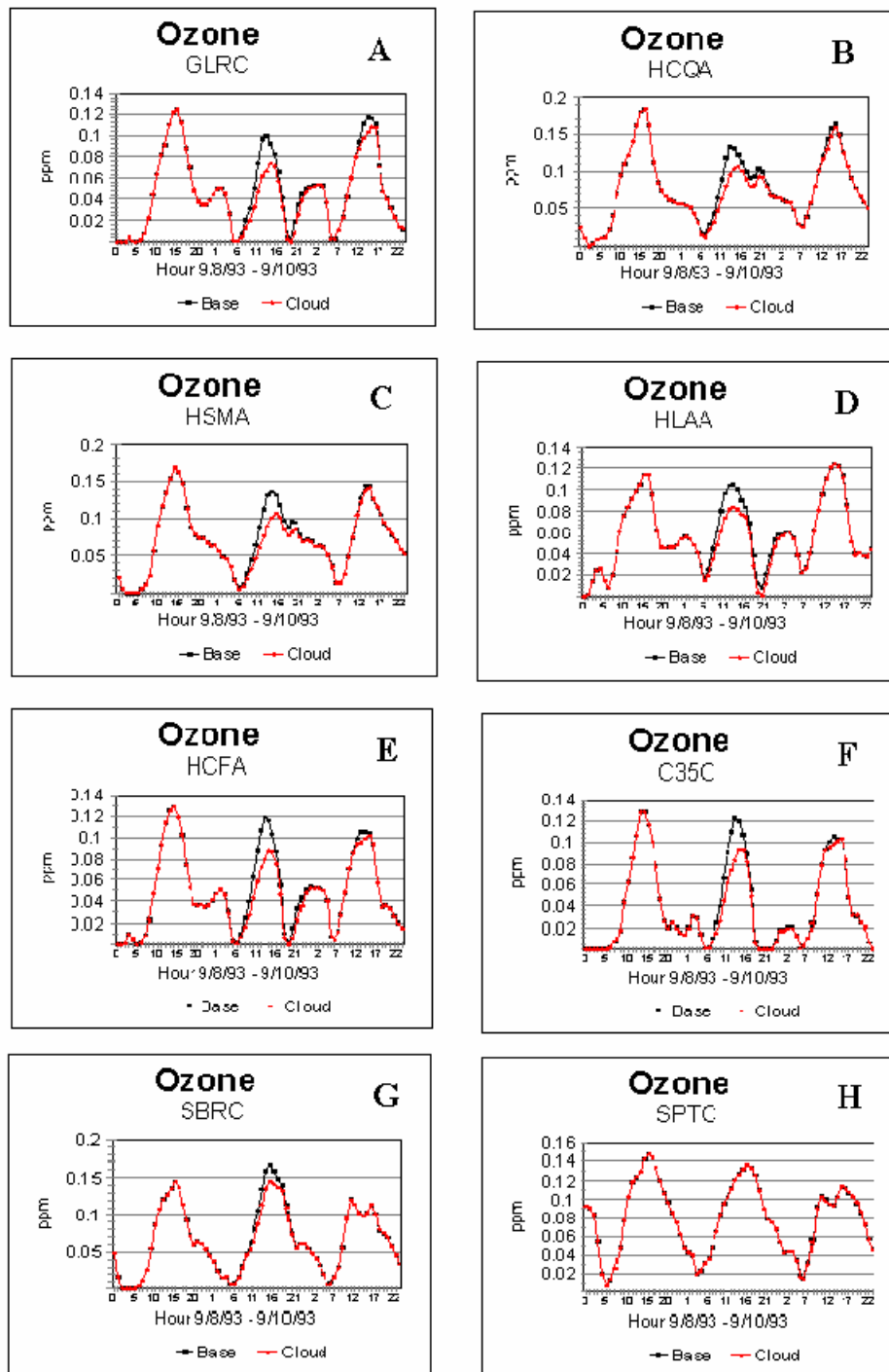


Figure 3-31. Time series of grid cell predicted ozone at selected monitoring sites for the base case and the cloud sensitivity simulation.

3.3 SPIKE INTENSITY

In this section, the spike intensity statistical results for the Houston area are presented for four cases: the base case, S5 (cloud cover), S7 (emissions upset at Chocolate Bayou and Texas City), and S12 (short duration emissions upset). Spike intensities were calculated using the method suggestion by Jolly (2001) from the CAMx model output and statistics generated using the SAS procedure UNIVARIATE (SAS, 2000). The statistics were calculated for both the fine and course grids over the same area. **Table 3-1** and **Table 3-2** show the results for the base case; **Table 3-3** and **Table 3-4** show the results for S5; and **Table 3-5** and **Table 3-6** show the results for S7. S12 is treated separately and presented later in this section.

Table 3-1. SAS moments and quantiles for the spike intensity for the base-case 16-km grid.

Moments	Values	Quantiles	Estimate
N	420	100% Max	24.5000
Mean	4.75215714	99%	15.0000
Std Deviation	3.15274206	95%	10.3330
Skewness	1.89579388	90%	8.2500
Uncorrected SS	13649.6278	75% Q3	6.2500
Coefficient of Variation	66.3433882	50% Median	4.0000
Sum Weights	420	25% Q1	2.5000
Sum Observations	1995.906	10%	1.5895
Variance	9.93978251	5%	1.2000
Kurtosis	6.34564169	1%	0.8460
Corrected SS	4164.76887	0% Min	0.4710
Std Error Mean	0.15383806		

Table 3-2. SAS moments and quantiles for the spike intensity for the base-case 4-km grid.

Moments	Values	Quantiles	Estimate
N	6720	100% Max	39.000
Mean	5.3301372	99%	20.500
Std Deviation	3.85791785	95%	12.600
Skewness	2.14814888	90%	10.000
Uncorrected SS	290920.076	75% Q3	6.833
Coefficient of Variation	72.3793349	50% Median	4.375
Sum Weights	6720	25% Q1	2.727
Sum Observations	35818.522	10%	1.667
Variance	14.8835302	5%	1.273
Kurtosis	7.83743769	1%	0.800
Corrected SS	100002.439	0% Min	0.412
Std Error Mean	0.04706178		

Table 3-3. SAS Moments and Quantiles for the spike intensity for S5 (clouds) 16-km grid.

Moments	Values	Quantiles	Estimate
N	420	100% Max	24.5000
Mean	4.69565476	99%	15.0000
Std Deviation	3.1153569	95%	10.2915
Skewness	1.97147348	90%	8.2085
Uncorrected SS	13327.2359	75% Q3	6.0000
Coefficient of Variation	66.345527	50% Median	4.0000
Sum Weights	420	25% Q1	2.5000
Sum Observations	1972.175	10%	1.6000
Variance	9.70544859	5%	1.1655
Kurtosis	6.84520718	1%	0.8000
Corrected SS	4066.58296	0% Min	0.4710
Std Error Mean	0.15201385		

Table 3-4. SAS Moments and Quantiles for the spike intensity for S5 (clouds) 4-km grid.

Moments	Values	Quantiles	Estimate
N	6720	100% Max	39.000
Mean	5.34482887	99%	21.500
Std Deviation	3.94798043	95%	12.600
Skewness	2.22534441	90%	10.000
Uncorrected SS	296697.58	75% Q3	6.833
Coefficient of Variation	73.8654225	50% Median	4.375
Sum Weights	6720	25% Q1	2.714
Sum Observations	35917.25	10%	1.600
Variance	15.5865495	5%	1.231
Kurtosis	8.11099252	1%	0.786
Corrected SS	104726.026	0% Min	0.412
Std Error Mean	0.04816043		

Table 3-5. SAS moments and quantiles for the spike intensity for S7 (upset) 16-km grid.

Moments	Values	Quantiles	Estimate
N	420	100% Max	25.5000
Mean	4.88902857	99%	19.5000
Std Deviation	3.39452337	95%	11.4585
Skewness	2.08393329	90%	8.4145
Uncorrected SS	14867.1407	75% Q3	6.2500
Coefficient of Variation	69.4314489	50% Median	4.1770
Sum Weights	420	25% Q1	2.5560
Sum Observations	2053.392	10%	1.6075
Variance	11.5227889	5%	1.2265
Kurtosis	6.77614338	1%	0.8460
Corrected SS	4828.04856	0% Min	0.4710
Std Error Mean	0.16563578		

Table 3-6. SAS Moments and Quantiles for the spike intensity for S7 (upset) 4-km grid.

Moments	Values	Quantiles	Estimate
N	6720	100% Max	39.0000
Mean	5.41456071	99%	22.0000
Std Deviation	4.00484527	95%	12.8000
Skewness	2.25397693	90%	10.0000
Uncorrected SS	304777.984	75% Q3	6.8750
Coefficient of Variation	73.9643617	50% Median	4.4440
Sum Weights	6720	25% Q1	2.7780
Sum Observations	36385.848	10%	1.6670
Variance	16.0387857	5%	1.2795
Kurtosis	8.29138198	1%	0.8000
Corrected SS	107764.601	0% Min	0.4120
Std Error Mean	0.04885411		

The spike intensity is calculated lower than those given by the monitoring stations for the 10-year period presented in Jolly (2001) over the Houston area from CAMx results for the three model cases investigated. This result is not totally unexpected as one considers that the grid cell size dilutes the effect. The effect of grid size on spike intensities can be seen by comparing the statistics for the two different grid sizes (16 km and 4 km) for the base case; for instance, the 100% maximum estimates of spike intensity differ by nearly 15 ppb. A monitoring station (a meter wide at best) would likely be more susceptible to recording large fluctuations due to transient ozone, and thus record greater spike intensities. Comparing the monitoring station values for only the days of the simulation may prove to be a better representation.

The four largest spike intensity values in the Houston area for the base-case model are 39, 35, 35, and 34 ppb, respectively, and are shown in **Figure 3-32**. These values all occur on September 8 and are dominated by 1- to 2-hr fluctuations. These plots show a characteristic spike above the base-line concentrations; and in three of the four plots, the ozone concentrations are well above 100 ppb when the spike occurs.

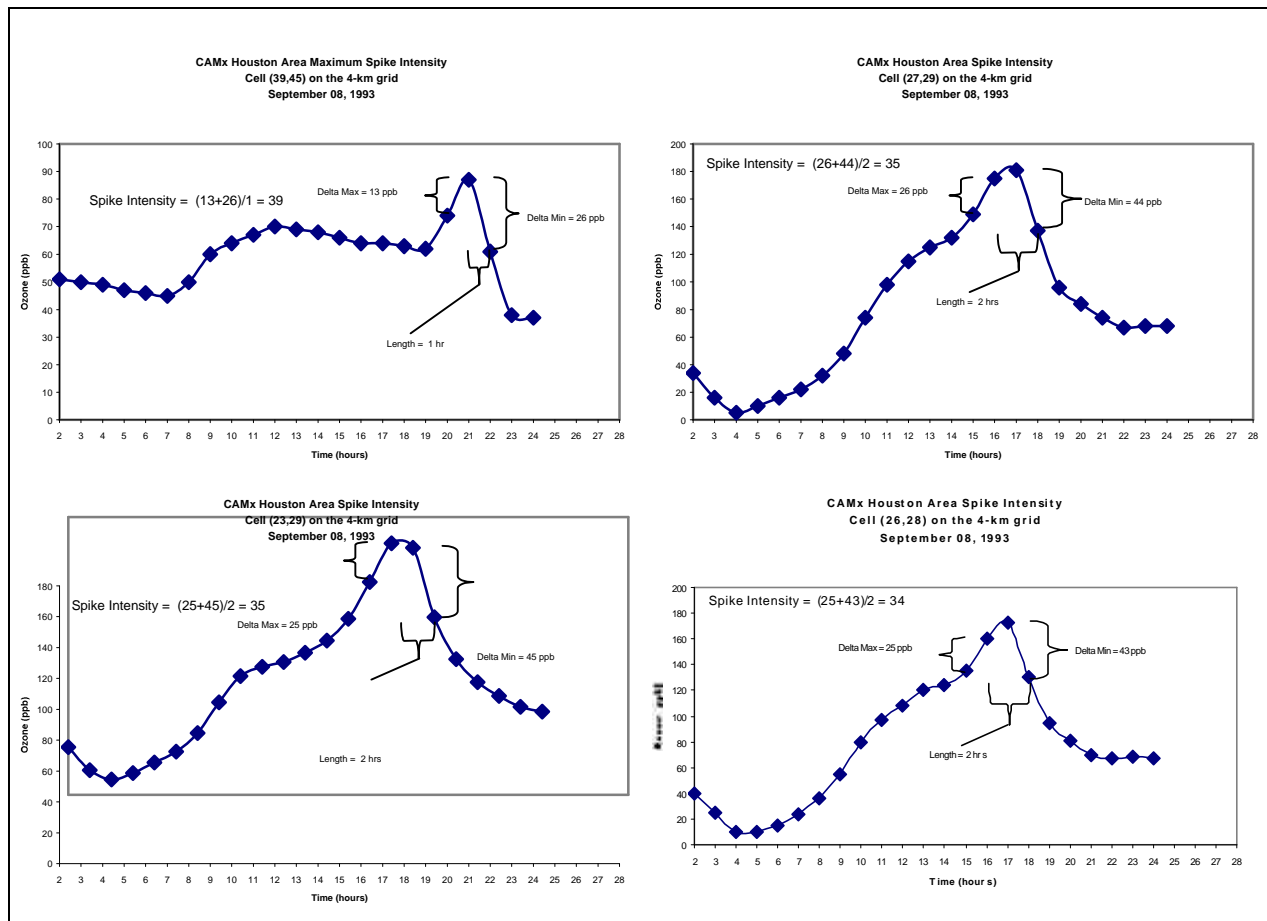


Figure 3-32. Four largest spike intensities calculated in the Houston area domain.

In addition to poor agreement with the monitoring station spike intensities, the model mean spike intensity responds only slightly to the different inputs as seen in the statistics between the base case and the two sensitivities. The mean spike intensity increases slightly for the two sensitivities. Thus, cloud cover variation during the day, as well as increased chemical output, may have some bearing on the spike intensity, but does not have a dramatic effect in the model runs. Likely, a more realistic study on the spike intensity would involve a very large fluctuating source of chemical upset, which is a possible area of future sensitivity simulations. Chemical upset should be more clearly defined; for S7 it was taken as 10 times, but perhaps 100 times the standard operating conditions is more realistic. On this note, one last sensitivity simulation was developed to investigate the effect on the spike intensity of a 2-hr fluctuation of 10 times more ethene and propene over standard operation from September 8 and September 10

at Chocolate Bayou. **Tables 3-7 and 3-8** show the base spike intensity statistics for those two dates only while **Tables 3-9 and 3-10** show the spike intensity statistics for S12.

Table 3-7. SAS moments and quantiles for the spike intensity for the base-case 16-km grid for September 8 and September 10.

Moments	Values	Quantiles	Estimate
N	140	100% Max	24.5000
Mean	6.23436429	99%	18.3330
Std Deviation	3.6604522	95%	13.2665
Skewness	1.46175451	90%	11.0665
Uncorrected SS	7303.87026	75% Q3	8.0000
Coefficient of Variation	58.7141211	50% Median	5.7750
Sum Weights	140	25% Q1	3.7025
Sum Observations	872.811	10%	2.1500
Variance	13.3989103	5%	1.5970
Kurtosis	4.08711719	1%	0.8570
Corrected SS	1862.44853	0% Min	0.8000
Std Error Mean	0.30936467		

Table 3-8. SAS moments and quantiles for the spike intensity for the base-case 4-km grid for September 8 and September 10.

Moments	Values	Quantiles	Estimate
N	2240	100% Max	39.0000
Mean	7.00692589	99%	23.3330
Std Deviation	4.5483717	95%	14.7500
Skewness	1.71376356	90%	12.7500
Uncorrected SS	156297.03	75% Q3	9.2250
Coefficient of Variation	64.9125132	50% Median	6.0000
Sum Weights	2240	25% Q1	3.7820
Sum Observations	15695.514	10%	2.2615
Variance	20.6876851	5%	1.6670
Kurtosis	5.47401313	1%	0.9290
Corrected SS	46319.7269	0% Min	0.5500
Std Error Mean	0.09610189		

Table 3-9. SAS moments and quantiles for the spike intensity for S12 (2-hr upset) 16-km grid for September 8 and September 10.

Moments	Values	Quantiles	Estimate
N	140	100% Max	24.5000
Mean	6.23786429	99%	18.3330
Std Deviation	3.65713577	95%	13.2665
Skewness	1.4629159	90%	11.0000
Uncorrected SS	7306.60836	75% Q3	8.0000
Coefficient of Variation	58.6280112	50% Median	5.7750
Sum Weights	140	25% Q1	3.7025
Sum Observations	873.301	10%	2.1500
Variance	13.374642	5%	1.5970
Kurtosis	4.10351565	1%	0.8570
Corrected SS	1859.07524	0% Min	0.8000
Std Error Mean	0.30908439		

Table 3-10. SAS moments and quantiles for the spike intensity for S12 (2-hr upset) 4-km grid for September 8 and September 10.

Moments	Values	Quantiles	Estimate
N	2240	100% Max	39.000
Mean	7.01038348	99%	23.333
Std Deviation	4.5353901	95%	14.750
Skewness	1.70673767	90%	12.750
Uncorrected SS	156141.568	75% Q3	9.250
Coefficient of Variation	64.695321	50% Median	6.000
Sum Weights	2240	25% Q1	3.800
Sum Observations	15703.259	10%	2.273
Variance	20.5697633	5%	1.667
Kurtosis	5.45628442	1%	0.929
Corrected SS	46055.7001	0% Min	0.550
Std Error Mean	0.09582761		

Again, no substantial effect on the domain-wide statistics occurs between the base case and S12. There are small increases in the overall statistics indicating that the spike intensity is only affected locally around Chocolate Bayou; therefore, no large transient chemical reaction is set up to increase the spike intensity domain-wide (**Figure 3-33**). As shown in Figure 3-33 the initial upset at 1000 creates increases in ozone concentration locally at Chocolate Bayou in comparison to the base case (the plots shown indicate the difference between S12 and the base case). The maximum difference in ozone concentrations between the base case and the sensitivity run occurs at 1100 CST on September 10; however, shortly after the upset is turned off at 1200 CST, the differences dwindle locally. Then, afternoon transport moves the ozone plume away from Chocolate Bayou slowly to the northwest; and during transport, the plume

dissipates, becoming smaller in size with changes in ozone along its path of around 2 ppb. The 2-ppb change moving into regions of 100 to 160 ppb has little effect on the spike intensity.

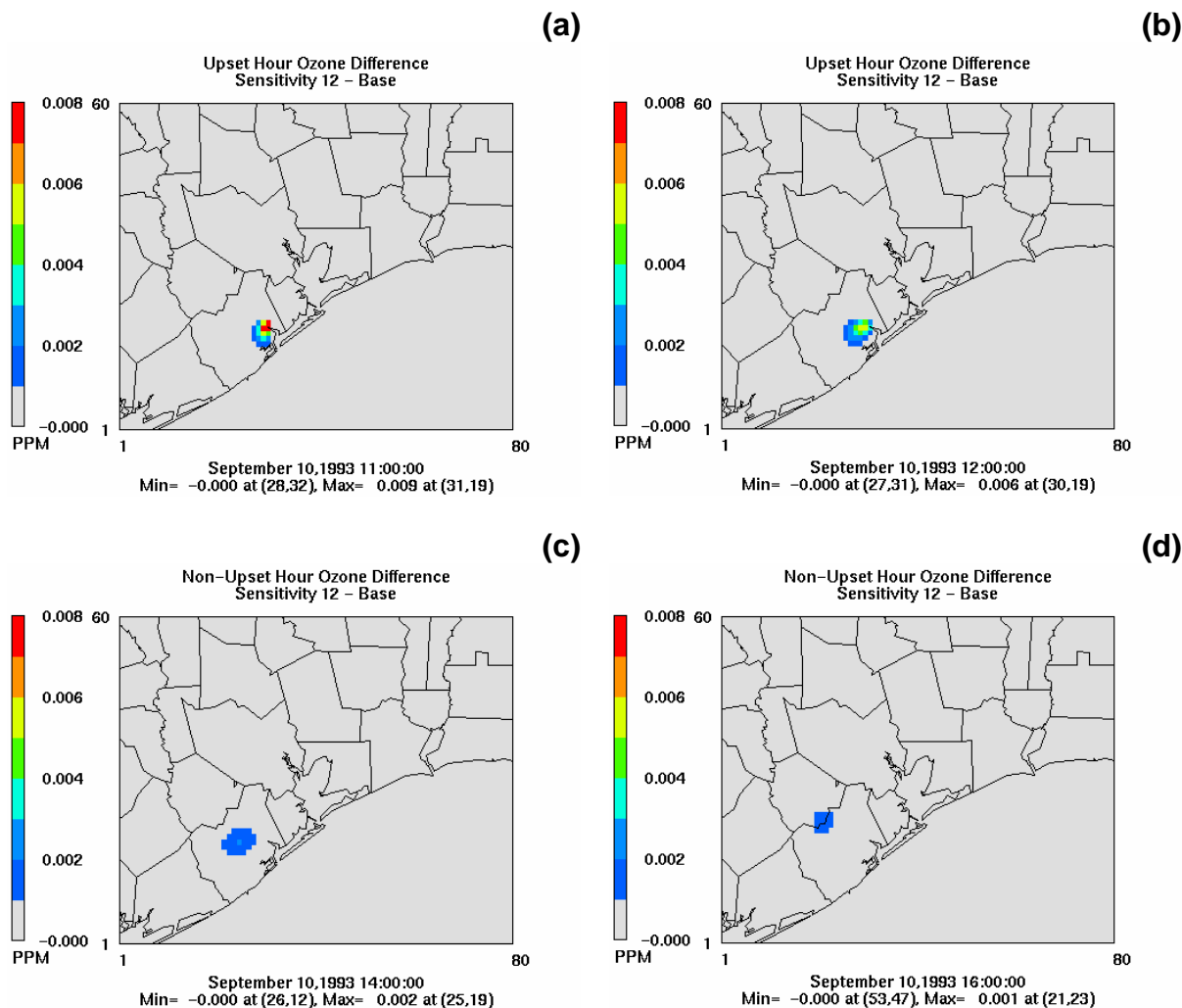


Figure 3-33. S12 upset from 1000 to 1200 CST at Chocolate Bayou on September 10, 1993 showing ozone differences from the base case at (a) 1100 CST, (b) 1200 CST, (c) 1400 CST, and (d) 1600 CST.

An interesting note is that the conditions on September 8 and September 10 show a greater mean spike intensity than the mean for the entire six days of the simulation (comparing Tables 3-1 and 3-2 to Tables 3-7 and 3-8). On those days the mean spike intensity is 2 to 3 ppb higher than for all six days indicating these days are more dynamic.

4. DISCUSSION

4.1 SOURCE CONTRIBUTIONS TO PEAK OZONE CONCENTRATIONS

NO_x emissions from both the urban core of Houston and the Ship Channel appear to be significant contributors to the peak ozone concentrations predicted by CAMx as do hydrocarbon emissions from the Houston Ship Channel. Sensitivity to hydrocarbon emissions from the urban core was not tested in this study but previous sensitivity simulations performed by MCNC and TNRCC (Wheeler et al., 1999) indicated that the ozone peak was also sensitive to urban hydrocarbon emissions. The response of CAMx to these emissions sensitivities indicates that peak ozone concentrations predicted to the southwest of Houston on September 8 and west of Houston on September 10 are largely due to both NO_x and hydrocarbon emissions from both urban and industrial sources.

Based on sensitivity simulations S1 and S3, it is evident that the W.A. Parish Power Plant does not have a large effect on the peak ozone concentrations in the September 6 through 11 simulation nor the peak ozone response to domain-wide NO_x emission reductions. The effect of the plant is local and in the direction of transport, which is away from Houston during most simulation hours.

In preparing the emission inputs for the various sensitivity simulations, STI had the opportunity to review the spatial, temporal, and chemical allocation of emissions in the modeling domain. In general, the spatial, temporal, and chemical distributions of anthropogenic and biogenic emissions were reasonable. The largest emissions of ethene and propene were found in the vicinity of the Houston Ship Channel and at chemical facilities along Galveston Bay and the Gulf Coast. Diurnal profiles of emissions were reasonable although many industrial areas showed minor increases of emissions on the weekend. These weekend increases are not understood and should be investigated further. No major errors in the processing of emissions for input to CAMx are evident. However, this does not mean that the underlying emission factors, temporal profiles, and speciation profiles are correct.

4.2 TRANSPORT AND DIFFUSION

Transport and diffusion are both mechanisms that can affect ozone concentrations. When horizontal transport is decreased, stagnation of the air results with the possible build-up of concentrations locally. Likewise, decreased vertical diffusion will allow concentrations to remain near the ground. The sensitivity simulation where vertical diffusion was reduced showed little impact on ozone concentrations. However, it may play a more important role in the application of CAMx when the wind fields, including vertical velocities, are more accurately represented and its affect should be evaluated in the development of any new CAMx simulations.

The peak ozone concentrations predicted to the southwest of Houston on September 8 and west of Houston on September 10 appear to be displaced from observed locations due to transport errors. Animations of ozone and ozone precursors indicate that ozone production begins in the urban and industrial areas surrounding Houston, and the production activity is advected to the peak locations as the day progresses. This is most evident on September 8 when

the peak ozone is displaced westward resulting in the overprediction at Croquet and an underprediction at Smith Point.

4.3 CLOUD COVER EFFECTS

Cloud cover can play a significant role in the photolysis rates in ozone formation. In the case of September 8 through September 10, the cloud cover acted to reduce the ozone concentration domain-wide when present. On September 8, there was little change as there were few clouds. The peak concentrations were reduced as much as 20 ppb on September 9, indicating a significant over-prediction on this day without including cloud cover. On September 10, there was a modest decrease of 4 ppb on the peak concentration due to the clouds. While the effects of clouds do not significantly impact the model's response to domain-wide NO_x emission reductions as shown by S7, cloud cover does explain some of the day-to-day variation in model performance for this episode.

4.4 SIMULATION OF UPSETS

An emissions upset on the order of ten times normal operation at chemical plants near Chocolate Bayou and Texas City was simulated. The simulation resulted in a large increase in ozone near the chemical plants. However, it did not significantly affect peak concentrations in Houston area. When the same upset conditions were simulated with reduced wind speeds as in S10, local ozone production at Chocolate Bayou and Texas City was enhanced further. Reducing the vertical diffusion coefficient by 25% did not have a great effect on the peaks but did increase the extent of high ozone concentrations. The sensitivity simulation performed show that CAMx is capable of simulating emissions upsets. However, due to limitations in the version of CAMx used, the actual ozone production rates and efficiencies could not be assessed for these simulations and compared to measurements made during the Texas 2000 Air Quality Study. To fully assess CAMx's ability to simulate emissions upsets, these upset conditions should be simulated with a version of CAMx that includes process analysis when available.

4.5 SIMULATION OF SPIKE INTENSITY

The spike intensities calculated for the model results were much lower than those presented by Jolly (2001) for historical monitoring data. A possible reason for these differences is the grid size in the model in comparison to a monitoring station. Model results are an average over the grid cell, which tends to remove some of the variations that might be expected at a point location. A comparison of spike intensity statistics between the 16-km and 4-km simulations shows that the spike intensities were even lower for the 16-km results. The various sensitivity runs showed little variation in the spike intensity statistics. Small increases in the mean spike intensity were seen for increased hydrocarbon release and increased cloud cover. The statistics for the spike intensity indicate that September 8 and September 10 had greater spike intensities than the other days. September 8 had the four greatest spike intensities, and the conditions on these days may provide insight into what creates bigger spike events. It appears that CAMx is capable of simulating the effects of upset emissions but cannot simulate the range of spike

intensities that have been historically observed. However, we do not know if the historical range of observed spike intensities are comparable to those observed for this episode alone.

Spike intensity is reduced if there is large decrease in ozone during nighttime titration that is greater than any decrease during the day because of the length of time between the maximum and minimum increases (**Figure 4-1**). In Figure 4-1, if the first decrease is taken, the length is five hours, and the spike intensity becomes 11 rather than 6.5. This could be addressed with a routine which chooses the first decrease after the maximum increase, or calculates the spike intensity for the top three decreases after the maximum increase and selects the highest. Likewise, the spike intensity as defined does not indicate an order to the minimum or maximum delta. Ideally, transient high ozone is best represented by a maximum increase followed by the maximum decrease. The routine used to evaluate the spike intensity for September 6 through September 10 indicated that approximately 30% of the cells had the maximum decrease before the maximum increase in the 24-hr period for each day. An example of such an occurrence is shown in **Figure 4-2**. These issues suggest that a stricter definition of spike intensity may be required to properly characterize rapid transient high ozone events.

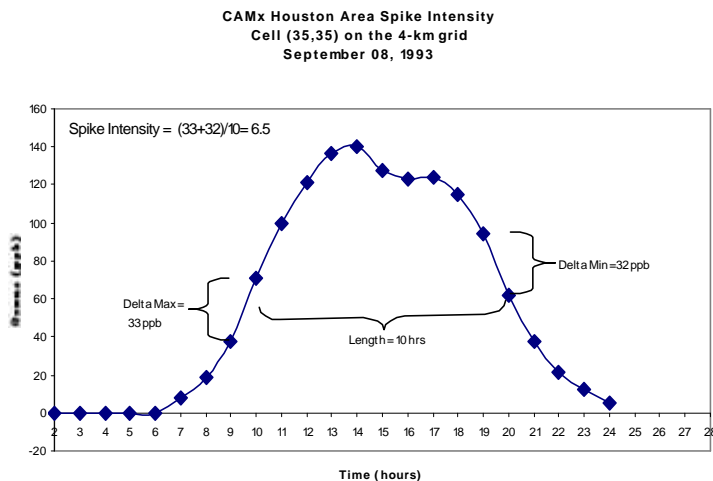


Figure 4-1. The spike intensity can be reduced when the minimum occurs during the nighttime due to titration.

CAMx Houston Area Spike Intensity
Cell (49,26) on the 4-km grid
September 08, 1993

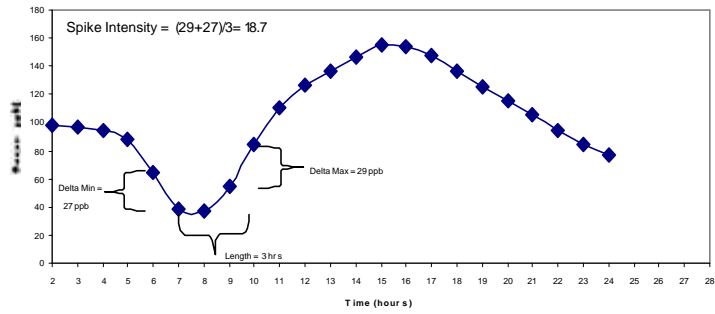


Figure 4-2. The greatest negative change occurs before the maximum positive change in this case and is not necessarily representative of a transient high ozone event.

5. CONCLUSIONS AND RECOMMENDATIONS

In general, CAMx responded as expected to changes in the input parameters with regard to the basic chemical and physical processes associated with ozone formation, transport, and diffusion. When hydrocarbon emissions are increased, ozone concentrations increase. When NO_x emissions are reduced, ozone concentrations decrease during the daytime hours and increase during the night over the urban core due to reduced titration of ozone. Likewise, the model responded to changes in the meteorological inputs in a manner consistent with our understanding of transport and diffusion processes. Based on an analysis of the base case and 12 sensitivity simulations performed, we conclude that

- The peak ozone concentrations predicted to the southwest of Houston on September 8 and west of Houston on September 10 were a result of both NO_x and hydrocarbon emissions from regions dominated by both mobile and industrial sources.
- The peak ozone concentrations predicted for September 8 and September 10 appear to have been displaced from observed locations due to transport errors. The transport errors are a result of the wind field inputs to CAMx.
- The W.A. Parish Power Plant did not have a large effect on peak ozone concentrations in the September 6 through 11 simulation and did not significantly affect the model's response to domain-wide NO_x emission reductions.
- Increased hydrocarbon emissions in the Houston Ship Channel could have produced significant increases in predicted ozone concentrations in the central Houston area on September 11 when central Houston was directly downwind of the Ship Channel. Underestimated emissions of ethene and propene in the Ship Channel could explain poor model performance for the August 1993 HGA episode when high concentrations of ozone were reported downtown.
- The inclusion of cloud cover in the CAMx inputs can significantly influence ozone production. However, the inclusion of cloud cover did not significantly affect the model's response to domain-wide NO_x reductions for this episode.
- An emissions upset on the order of ten times normal operation can be simulated with CAMx resulting in significant ozone production increases in the proximity of the upset source. However, the simulation of such upsets at Chocolate Bayou and Texas City did not significantly affect the predicted peak ozone concentrations in the Houston area for this episode.
- A simulated wind speed reduction of 25% could significantly increase peak ozone concentrations within the Houston area and affect the spatial distribution of high ozone.
- Reduced wind speeds in combination with an emissions upset at Chocolate Bayou and Texas City could significantly enhance the CAMx-simulated ozone production in the vicinity of the upset.
- Reducing the vertical diffusion coefficient by 25% did not have a great effect on the peaks but increased the area extent of high ozone concentrations.

- Spike intensities calculated from CAMx simulations are much lower than those calculated from historical monitoring data. However, it is not known if the historical range of observed spike intensities are comparable to those observed for this episode alone.

Based on the results of this study the following recommendations are made:

- Further investigations of the quantity, speciation, and temporal allocations of emissions from chemical industry sources should be carried out.
- Cloud cover should be included in future CAMx simulations for episodes when significant cloud cover is reported.
- Special attention should be paid to the development and evaluation of wind fields for any future CAMx modeling.
- CAMx with process analysis should be applied to the HGA, which will allow the determination of actual ozone production rates in the modeling system.
- The SAPRC chemical mechanism should be evaluated for the HGA modeling and used to assess the ability of CAMx to simulate high ozone in the urban core of Houston and emission upset-related ozone events.
- The method of calculating spike intensity should be re-evaluated and potentially re-designed to better capture the types of rapid ozone formation events for which it was intended.
- Episode-specific spike intensities should be calculated from observations for comparison with model results.

6. REFERENCES

- ENVIRON (1998) Comprehensive Air Quality Model with extensions (CAMx), User Guide. ENVIRON International Corporation, Novato, CA, December.
- Hess M., Koepke P., and Schult I. (1998) Optical properties of aerosols and clouds: The Software Package OPAC. *Bull. Amer. Meteor. Soc.*, **79**, 831-844.
- Jolly J. (2001) Analyzing “spikiness” in diurnal ozone patterns in Houston: a case study involving upset emissions. Texas Natural Resource Conservation Commission presentation, May.
- Rasband W. (2000) *Image J* **1**, 18. <<http://rsb.info.nih.gov/ij/index.html>>.
- SAS (2000) SAS Procedures Guide, Version 8. SAS Publishing, Cary, NC, 1563 pp.
- Thorpe S., Ambrosiano J., Balay R., Coats C., Eyth A., Fine S., Hils D., Smith T., Trayanov A., Turner T., and Vouk M. (1996) The Package for Analysis and Visualization of Environmental Data. *1996 Fall Proceedings, Thirty-eighth Semi-Annual Cray User Group Meeting, Charlotte, NC, October 14-18*.
- Wheeler N., Arunachalam S., Dolwick P., and Vukovich J. (1999) Evaluation of control strategies for the Houston Galveston area. Report prepared for Texas Natural Resource Conservation Commission, Austin, TX by North Carolina Supercomputing Center (MCNC), Environmental Programs, Research Triangle Park, NC, Work Order No. 9800693000-07, June.